

Response to reviews for acp-2018-13333

We are thankful to Dr. Ian Chang and the anonymous referee for evaluating this manuscript and helping us to improve its quality with their feedback. Please, find below our responses to reviewer comments, with our responses in black text.

Ian Chang (Referee)

Received and published: 8 February 2019

Dear Editor:

This manuscript outlines a technique to simultaneously retrieve above-cloud aerosol optical properties and underlying cloud properties from Meteosat Second Generation (MSG) Spinning Enhanced Visible and Infrared Imager (SEVIRI) over the southeast Atlantic. This work demonstrates a cogent pathway for estimating the aerosol direct radiative effects in the southeast Atlantic by using high temporal resolution data to synchronously evaluate diurnal cycles of aerosol and cloud properties. Overall, this paper is concisely and coherently written with minor technical issues. Thus, I support the publication of this manuscript in the Special issue of Atmos. Chem. Phys. upon addressing the comments and suggestions.

Best regards,
-Ian Chang

General Comments:

The criteria for rejecting aggregated retrievals using standard deviations of AOT and inhomogeneity parameters of CER to remove high AOT uncertainty grids are performed to ensure that the accepted retrievals are reliable. However, such filtering would discard some reliable pixels. I suggest the authors discuss the number of cloudy pixels that are removed using this filtering technique since removing an excessive number of cloudy pixels may have a significant impact on estimating the above-cloud aerosol direct radiative effects. Also, have the authors tested the filtering at finer grid resolutions in order to retain a higher number of reliable retrievals? Despite the remarks, I anticipate that Part 2 of this manuscript will elaborate on these points.

The filters described in the manuscript have been implemented in order to ensure that the measurements have been performed in optimum conditions for the retrieval. The LUT has been computed with a 1D radiative transfer code. At cloud edges and for inhomogeneous clouds, the independent pixel approximation is not valid and the plane-parallel bias is not negligible. Therefore, the retrieval of the aerosol and cloud properties becomes unstable, and using those data could lead to significant errors in the estimation of the above-cloud aerosol direct radiative effect. Removing those observations allows us to improve the quality of the final products. For the case study described in the manuscript (28/08/2017 at 10:12 UTC), those removed observations represent 23.7% of the pixels. Figure 1 in this document shows the AOT retrieved above clouds together with the filtered pixels in magenta. We note that while removing these pixels is not ideal when comparing to e.g. GCM model studies, by clearly stating our assumptions, GCM studies can perform a similar screening procedure.

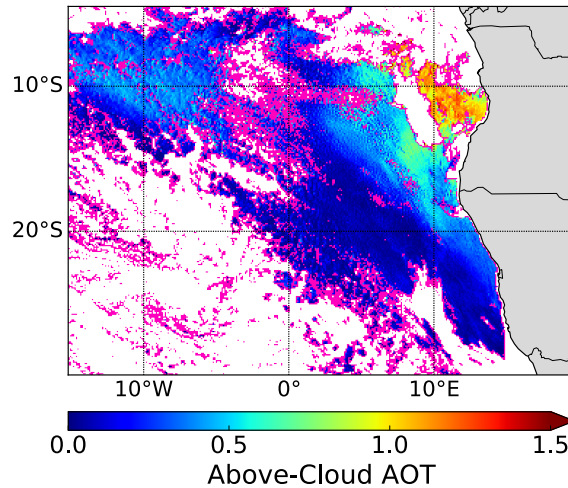


Figure 1: Above cloud AOT at 550 nm retrieved from SEVIRI measurements on the 28 August 2017 at 10:12 UTC over the SEAO. Pixels in magenta correspond to pixels removed with the cloud edge and cloud heterogeneity filters.

A major objective of this paper addresses the sensitivity of retrievals due to aerosol model assumptions. This analysis is presented using a case study from 28 August 2017 at 1012 UTC. Since this paper aims to demonstrate the validity of simultaneous above-cloud AOT and underlying COT retrievals throughout the day, a sensitivity analysis should be presented at different times of the day instead of only at a particular time of the day. Hence, the authors should present these details during other hours of the day (unless the uncertainty variations are negligible throughout the day) if there are sufficient time and space to consolidate this information. Alternatively, the authors need to explicitly indicate that this uncertainty estimate is limited to a case study and discuss the anticipated uncertainties during other times of the day. The abstract should state the ranges of modified parameters that are used to conduct the sensitivity analysis and mention the time period that the uncertainties represent.

The entire Section 3c has been modified. The evolution of the sensitivity of the retrieval to the aerosol model assumptions during the day has been analysed. The uncertainty on the cloud properties remains small all day long (lower than 5.6% for the COT and 2.6% on the CER), with the sensitivity of the COT being slightly smaller in the middle of the day. We also show that the uncertainty on the retrieved AOT and AAOT is smallest during the 09:00-15:00 UTC time period. The following analysis has been added to Section 3c:

The variation of the solar zenith angle, and therefore, of the satellite observation geometry during the day can impact the sensitivity of the retrieval to the aerosol assumptions. Therefore, the 15-minute SEVIRI observations for the 28 August have been processed using the eight aerosol models described above and compared to the aerosol and cloud properties retrieved with the CLARIFY aerosol model. The difference Δx_i of a product x is defined as:

$$\Delta x_i = (x_{\text{CLARIFY}} - x_i) / x_i \times 100\%$$

where x_{CLARIFY} and x_i is the mean product x retrieved over the SEVIRI slot with the aerosol CLARIFY model and the modified model i , respectively. Figure 11 shows the time series of ΔAOT (a), ΔAAOT (b), ΔCOT (c) and ΔCER (d) obtained with the modified aerosol models. The sensitivity of the retrieved cloud properties to the aerosol model assumptions remains small (lower than 5.6% for the COT and 2.6% for the CER) and dominated by the sensitivity

to g . Apart from a small decrease of ΔCOT at midday when g is overestimated (solid blue line) and an increase of ΔCOT in late afternoon when the SSA is underestimated (solid red line), no significant trend is observed on the cloud property sensitivities. As observed previously, the uncertainty on the AOT is led by the SSA assumption, with the AOT being overestimated (respectively underestimated) when the assumed SSA is overestimated (respectively underestimated). Until 15:00, ΔAOT stays within $\pm 40\%$, with the sensitivity to the SSA being slightly larger at midday. Then it increases up to 60% when the SSA is overestimated and g is underestimated (dashed blue line). Similar trends are observed on $\Delta AAOT$, with generally lower values than ΔAOT . An increase of the uncertainty is observed on the AAOT after 15:00, that reaches up to 27% at 16:30. Before 15:00, there is a larger AAOT sensitivity to the SSA around midday ($+8.9\%/-15.2\%$), but there is no evident evolution of the sensitivity to g with time. The case that lead to the largest biases on the AAOT is when the SSA is underestimated and g overestimated (dashed green lines), with an underestimation of up to 23%. However, it should be noted that 0% of the AERONET observations used in Figure 8 are associated with an SSA lower than $SSA_{CLARIFY} - \sigma_{SSA}$ and a g larger than $g_{CLARIFY} - \sigma_g$. Otherwise, the sensitivity of the AAOT to the aerosol property assumptions stays between -16.6 and +9% before 15:00.

In conclusion, the retrieved AOT is less sensitive to the aerosol property assumption before 15:00, with an uncertainty of 40%. This uncertainty is dominated by the sensitivity of the retrieval to the SSA. An overestimation (respectively underestimation) of the AOT is expected when the observed aerosols are more (respectively less) absorbing than the aerosol model assumed for the retrieval. A better accuracy is obtained on the retrieved AAOT, with an uncertainty generally lower than 17 % before 15:00. The sensitivity of the cloud properties to the aerosol model assumption remain small all day long, with an uncertainty of 5.6% on the COT and 2.6% on the CER.

In the conclusion, the following text has been added:

Retrievals have been performed considering aerosol models with modified SSA and asymmetry factor g . It has been shown that the sensitivity of the retrieved cloud properties to the aerosol model assumption is small with errors lower than 5.6% on the COT and 2.6% on the CER. As expected the impact of the assumed aerosol properties is much larger on the above cloud AOT, with an uncertainty estimated at 40% before 15:00 UTC.

Finally, the comments about the sensitivity analysis in the abstract have been modified:

Between 09:00-15:00 UTC, an uncertainty of 40% is estimated on the above-cloud AOT, which is dominated by the sensitivity of the retrieval to the single scattering albedo. The absorption AOT is less sensitive to the aerosol assumptions with an uncertainty generally lower than 17% between 09:00-15:00 UTC. Outside of that time range, as the scattering angle decreases, the sensitivity of the AOT and the absorption AOT to the aerosol model increases. The retrieved cloud properties are only weakly sensitive to the aerosol model assumptions throughout the day, with biases lower than 6% on the COT and 3% on the CER.

Specific Comments:

Page 7 Lines 267-269: Is the negligible retrieval sensitivity associated with aerosol/cloud altitude assumptions quantified or is the negligibility a mere presumption? Both Jethva et al.

(2013) and Meyer et al. (2015) have quantified retrieval uncertainties associated with aerosol top height assumptions.

The Rayleigh scattering is expected to be small at the wavelengths used for the retrieval. A test has been made using new LUT, assuming a cloud top height at 3 km and an aerosol layer located between 4 and 5 km. An impact of 2.3% has been observed on the AOT and lower than 0.3% on the cloud properties. The following sentence has been added to section 2d:

We have evaluated the error due to the fixed aerosol and cloud altitudes to be lower than 2.5% on the AOT and 0.3% on the cloud properties.

Page 10 Lines 398-399: The above-cloud AOT retrievals are stable within two times the standard deviation of the retrievals but not necessarily stable within one standard deviation. Thus, it is only more stable relative to one standard deviation. I suggest the authors justify the validity of defining the stability with respect to two standard deviations.

The obvious benefit of geostationary SEVIRI retrievals over polar-orbiting satellite retrievals are that they are available every 15minutes. It is therefore relevant to examine whether the retrievals made at time $t=0$ and at time $t+15$ mins are similar; if they were not, then this would suggest that the retrieval algorithm is not stable. Note that this assumes that the scene is changing relatively slowly; cloud and aerosol optical depths should not vary between time $t=0$ and time $t+15$ minutes. Figure 13 indicates that outside of the glory regions, the retrieval algorithm does indeed appear to be stable; there is little variation from one time step to the next. We included the 2sd measure as a rough metric, but on reflection it adds little to our quantification of stability as we only applied this metric to the above cloud AOT. This is because there can be longer timescale trends in cloud and aerosol (indeed there is a shallow slope in the above cloud AOT for 06/09/2017 of around 0.02 to 0.03/hour), and these statistics would differ depending on the area chosen and the prevailing meteorological conditions. Therefore, we chose to remove this statistical analysis as it is too simplistic.

Technical Corrections:

Page 2 Line 84: “polar orbiting” => “polar-orbiting”

The correction has been applied.

Page 3 Line 89: “from satellite platforms than currently available” => from geostationary satellite platforms instead of polar-orbiting satellite platforms that have coarser temporal resolutions.

The sentence has been modified to:

Therefore, the study of the SEAO cloud and above-cloud aerosol optical properties would benefit from the high temporal resolution observations provided by geostationary satellite platforms.

Page 4 Line 160: “MODIS, and hence” => “MODIS. Hence, SEVIRI is significantly”

Page 5 Line 174: Remove “and” and “one”

Page 5 Line 212: “of hydration” seems redundant in this sentence.

Page 6 Line 220: “are” => “include”

Page 6 Line 255: “are close” => “are close to each other”

Page 7 Line 268: “due of” => “due to”

Page 7 Line 286: “around” => “approximately”

Page 7 Line 286: “observations” is vague in the context of this sentence. I suggest “pixels” as a more suitable word.

Page 8 Line 297: “on the 28” => “on 28”

Page 8 Line 334: “10% indicating” => “10%, indicating”

Page 9 Line 380: It would be helpful to mention that the uncertainty of each component is computed from the averaged absolute values between the positive and the negative biases of the modified parameter.

Page 10 Line 420: “from” => “for”

Page 11 Line 431: “polar orbiting” => “polar-orbiting”

Page 11 Line 435: “in” => “of”

Page 11 Line 439: “the” => “their”

Page 11 Line 441: “contribution” is a bit vague. I suggest replacing this term with “absorption” or a more definitive term.

Page 12 Line 485: “above cloud” => “above-cloud”

Page 18 Line 729: “Cloud optical thicknesses (COT) and aerosol optical thicknesses (AOT)” => “COTs and AOTs”

Page 18 Line 733: “COT and CER” => “COTs and CERs”

Page 18 Line 734: “absorbing aerosols above” => “overlying absorbing aerosols”

Page 20 Line 748: “ones” => “lines”

Page 21 Line 758: “composite” => “composite for”

Page 22 Line 779: Remove “the”

Page 24 Line 798: “ones” => “areas”

The above corrections have been applied.

Anonymous Referee #2

Received and published: 11 February 2019

General Comments:

The paper describes what looks to be a promising method to simultaneously retrieve above cloud aerosol optical depth with cloud optical depth and effective radius from the Spinning Enhanced Visible and InfraRed Imager (SEVIRI). While the technique used is not tremendously novel, the application to geostationary data appears so, and the recognition of the impact of varying water vapour in particular on the measured satellite signal and hence the retrieved quantities shows good insight.

My own feeling is that the paper is a little ‘thin’ and actually would have benefited from including some of the material that I anticipate will be in the companion manuscript. Moreover, even if some of these comparisons are included here, given the title I think the paper has to encompass or at least discuss the full range of likely sensitivities that could be present in order to either show more generalised utility or to identify when the method will work optimally. If this is done I see no reason why the work should not be published.

Specific remarks:

Some aspects of the methodology are not clear. I assume that in working out the aerosol model parameters you first fit the size distribution, then iteratively adjust the refractive indices until you fit the EXSCALABAR measurements of SSA, assuming that the biomass aerosols are spherical. Is this correct? If so I think you must: (a) provide some error bars on the size distribution and SSA observations in figure 4. These could then perhaps be used to give a realistic range in the size distribution parameters and the complex refractive index that you have selected. At the moment the reader has no feel whether it is sensible to try to match the EXSCALABAR data as well as you have. (b) justify the assumption of Mie scattering.

(a) Errors bars are now provided in Figure 4 in the manuscript and the following explanations have been added to Section 2c:

The uncertainty in SSA calculations are related to the corresponding uncertainties in the extinction and absorption coefficients measured by EXSCALABAR. This error analysis has been performed previously and the reader is directed to Davies et al. (2019). Briefly, the measured extinction has an accuracy of ~2%, and we use a 2% extinction uncertainty in the analysis here. The errors in absorption measurements using photoacoustic spectroscopy depend on uncertainties in the ozone calibration, microphone pressure dependence and the background response from laser scattering/absorption on the windows of the photoacoustic cell. We have shown in recent publications that our calibration uncertainties are ~5% (Cotterell et al. 2019; Davies et al. 2018), and the uncertainty in the pressure-dependent microphone response is 1.2% (Davies et al. 2019). The background response from laser-window interactions is ranging from 0.27 – 0.54 Mm^{-1} . Thus, the total absorption uncertainty, propagating all the above uncertainties, is absorption-dependent and ranges from 29.0 – 55.0 % (dependent on PAS measurement wavelength) at 1 Mm^{-1} and 8.1 % at 100 Mm^{-1} (independent of PAS measurement wavelength). We propagated these total measurement uncertainties for both extinction and absorption measurements to derive the standard deviation σ in our calculated SSA values. We find that the mean SSA uncertainties are 0.013 and 0.018 at the measurement wavelengths of 405 and 658 nm respectively.

Three sources of errors have been taken into account on the PCASP measurements: the error on the bin concentration is calculated according to Poisson counting statistics, the sample flow rate error is assumed to be 10% and a bin edge calibration error of half a bin has been considered.

The aerosol model is selected by iteratively adjusting the refractive index and fitting the PCASP measurements (Fig. 4a) until the aerosol model matches the SSA from EXSCALABAR (Fig. 4b).

The uncertainties on the aerosol properties have been estimated using the errors on the PCASP and EXSCALABAR measurements. The uncertainty on the imaginary part of the refractive index is 0.02 for the real part and 0.004 for the imaginary part. For the size distribution, the uncertainty is 0.016 μ m, 0.09 and 0.00045 for radius, the standard deviation and the number fraction of the fine mode respectively.

(b) Martins et al. have observed that smoke particles from biomass burning could be considered spherical one hour after being emitted, which justify the use of the Mie theory. The following sentence has been added to Section 2c:

The aerosol optical properties are calculated using the Mie theory, as the spherical approximation is expected to be valid for biomass burning particles from one hour after being released in the atmosphere (Martins et al., 1998).

Martins, J. V., Hobbs, P. V., Weiss, R. E., and Artaxo, P., Sphericity and morphology of smoke particles from biomass burning in Brazil, *Journal of Geophysical Research*, 103 (D24), 32051–32057, doi:10.1029/98JD01153, 1998.

Does EXSCALABAR extend further than 0.65 microns? This would give more confidence in the final aerosol model both in terms of the size distribution and complex refractive index at the longer SEVIRI channel wavelengths. The assumption of a fixed refractive index with wavelength seems quite large.

EXSCALABAR does not extend further than 0.65 μ m. However, shortwave irradiance spectra from 0.3 to 1.7 μ m were measured during the campaign with the SHIMS (Spectral Hemispheric Irradiance Measurements) instrument. The radiative closure using the CLARIFY aerosol model is being studied and a paper is currently in preparation. The assumption of a fixed refractive index with wavelength has been motivated by the relatively small contribution of aerosols from the coarse mode and therefore, by the small impact of aerosols on the satellite signal measured at 1.6 μ m. For the algorithm developed by Meyer et al. (2015), which uses a similar method and spectral bands at longer wavelengths, the aerosol refractive index is also assumed to be spectrally invariant.

Meyer, K., Platnick, S., and Zhang, Z.: Simultaneously inferring above-cloud absorbing aerosol optical thickness and underlying liquid phase cloud optical and microphysical properties using MODIS, *Journal of Geophysical Research: Atmospheres*, 120, 5524–5547, <https://doi.org/10.1002/2015JD023128>, 2015.

You seem to assume a fixed aerosol and cloud layer height. Is this realistic and what impact does it have if the 'real' heights are different (i.e. did you actually investigate the impact of varying these heights – you imply it is negligible)?

Next to the coast, where the AOT is usually the largest, the cloud top derived from CALIOP and CATS is usually around 1 km (Rajapakshe et al., 2017). It slightly rises to the west, reaching 1.5/2.0 km at 19W. The satellite observations indicate that the bottom of the aerosol layer is within 2 and 3.5 km and the top is between 3 and 5 km. However, the Rayleigh scattering is expected to have a small contribution to the signal at the wavelength used for the retrieval. The influence of the fixed aerosol and cloud altitudes has been investigated by processing new LUT with a cloud top height at 3 km and an aerosol layer located between 4 and 5 km. The impact of the AOT is estimated to be lower than 2.5% and the impact on the cloud properties is lower than 0.3%. The following sentence has been added to section 2d:

We have evaluated the error due to the fixed aerosol and cloud altitudes to be lower than 2.5% on the AOT and 0.3% on the cloud properties.

Rajapakshe, C., Zhang, Z., Yorks, J. E., Yu, H., Tan, Q., Meyer, K., ... & Winker, D. M. Seasonally transported aerosol layers over southeast Atlantic are closer to underlying clouds than previously reported. *Geophysical Research Letters*, 44(11), 5818-5825, 2017.

It is good that you have investigated the impact of variations in humidity on the retrievals via your correction process but you are limited to the baseline set of atmospheres contained in the case study you have selected. Are the retrieval errors likely to be of the same order of magnitude if these conditions change? Or how sensitive are you to both the total amount and vertical distribution of water vapour? What about uncertainty in the cloud top height (line 180)? I believe it is quite challenging to (a) detect and (b) accurately locate low cloud over ocean using thermal IR radiances.

In the companion paper, a section will be dedicated to the validation of the atmospheric correction scheme. The water vapour profiles from the forecast have been compared with the dropsonde measurements from the CLARIFY campaign. Figure 2 in this document shows comparison of the column integrated water vapour. In order to be consistent with the atmospheric correction scheme, the integration of the forecasted water vapour above cloud is done based on the cloud top height retrieved by SEVIRI. Note that the measurements from the CLARIFY dropsondes have not been assimilated in the forecast model. In general, there is a relatively good agreement between the observations and the forecast, especially above clouds. We have also looked at the tephigrams obtained from the forecast and the measurements. An example is shown in Figure 3 of this document. A good consistency is generally obtained for the vertical distribution of the water vapour. On the analysed profiles, we have observed that the cloud top heights retrieved by SEVIRI using the thermal IR radiances are consistent with the altitude of the temperature inversion from the forecast model.

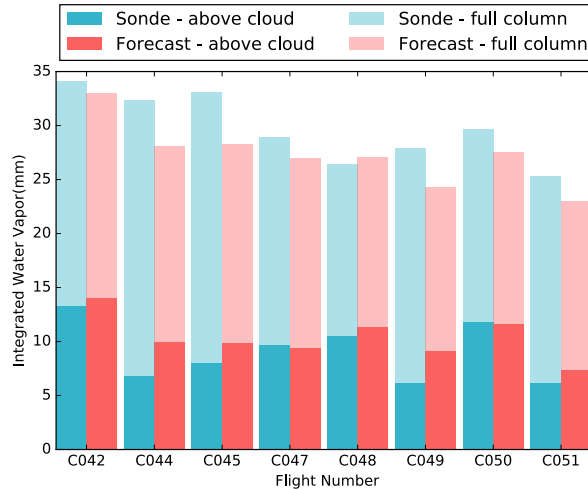


Figure 2: Comparison of the above cloud and the full column integrated water vapour from the dropsondes and from the NWP forecast.

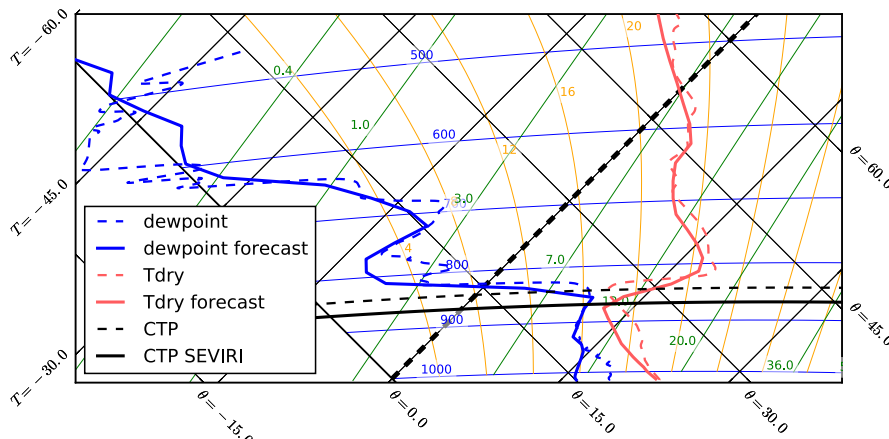


Figure 3: Tephigram obtained from the dropsonde (dashed lines) and the forecast (solid lines) for the flight C051 of the CLARIFY campaign.

Similarly, are you sure that you have considered a wide enough variation in aerosol model parameters? You don't really justify the choices that are made for the perturbations applied. Lines 364 and 365 imply that there should be a variation in the aerosol properties in the study region but you don't tie these to the perturbations you have implemented.

We have modified the analysis of the sensitivity of the retrieval to the aerosol assumption. Instead of analysing the sensitivity to the aerosol size distribution and refractive index separately, we considered a range of SSA and asymmetry factor g that is consistent with observations from AERONET. The choice of the variation in aerosol model parameters and the result of the sensitivity analysis read as follows:

In order to create a range of aerosol optical properties, a thousand aerosol models have been processed using the Mie theory. The radius and the standard deviation of the fine mode, and the real and imaginary part of the refractive index of the models are random values following a normal distribution. Their mean corresponds to the CLARIFY model values provided in Table 1, with standard deviations of $0.01\mu\text{m}$ and 0.1 for the radius and the standard deviation of the

fine mode, 0.02 for the real part of the refractive index and 0.008 for the imaginary part. Figure 8a and 8b show the histograms of the simulated SSA and asymmetry factor g at $0.55 \mu\text{m}$ in orange. As a comparison, histograms of the AERONET SSA and g are plotted in blue. The data corresponds to the AERONET level 2.0 retrievals for August-September, from 1997 to 2018 and for inland sites of Southern Africa (10°S – 35°S , 10°E – 40°E). Only data associated with an Ångström exponent larger than 1.0 have been used in order to remove measurements dominated by coarse mode particles (such as dust and sea salt) that are less likely to be observed above clouds in the SEAO. The mean SSA (0.862) and the mean g (0.620) from AERONET are respectively slightly larger and smaller than the CLARIFY model. Small differences between above-cloud and full column aerosol properties could be explained by the contribution of aerosol within the boundary layer, such as pollution, desert dust and sea salt. The dashed lines in Figure 8a and 8b represent the mean \pm the standard deviation of SSA and g . The AERONET standard deviation is 0.023 for the SSA and 0.024 for g while the simulation produces a standard deviation of 0.036 for the SSA and 0.041 for g . The simulated range of both optical properties is larger than the range observed by AERONET. Therefore, the variation of the aerosol microphysical properties used for the simulations is wide enough to cover the range of observed aerosol optical properties.

From the simulated standard deviation σ of g and SSA, eight aerosol models have been defined and their properties are summarized in Table 2. The first four are used to test the sensitivity of the retrieval to g and SSA independently ($[SSA_{\text{CLARIFY}} \pm \sigma_{\text{SSA}}, g_{\text{CLARIFY}}]$ and $[SSA_{\text{CLARIFY}}, g_{\text{CLARIFY}} \pm \sigma_g]$) and the sensitivity to both parameters will be assessed with the last four ($[SSA_{\text{CLARIFY}} \pm \sigma_{\text{SSA}}, g_{\text{CLARIFY}} \pm \sigma_g]$). New LUTs have been processed with these modified aerosol models and used to re-process the case study from section 3.a. After aggregating the data on a $0.1 \times 0.1^\circ$ grid, the AOT as well as the Absorption AOT (AAOT), the COT and the CER are compared against those obtained with the standard CLARIFY-2017 aerosol model. Results are shown in Figure 9 and 10. For each aerosol and cloud property, a linear relationship is observed between the retrieval using the standard CLARIFY-2017 aerosol model and the modified one. The retrieval of cloud properties (fig. 9c, 9d, 10c and 10d) appears to be weakly sensitive to the assumed aerosol model, with g having a slightly larger impact. On average, differences lower than 4.1% are observed on the COT and lower than 2.4% on the CER. As expected, the choice of the aerosol model has much more influence on the AOT retrieval. The uncertainty on the AOT is dominated by the SSA assumption. When aerosols are more absorbing than the CLARIFY model, the algorithm overestimates the AOT by 25.7%. Conversely, the retrieved AOT is underestimated by 32.6% when aerosols are less absorbing than the CLARIFY model. The impact of g alone on the retrieved AOT is far less significant and lower than 4.3%. Figure 9a, which shows the impact of a perturbation on both the SSA and g , confirms that the SSA is the parameter with the strongest influence on the AOT retrieval. The largest overestimation (27.5%) is observed when both the SSA and g are overestimated (fig. 10a), while the largest underestimation (-33.3%) is obtained when the SSA is underestimated and g is overestimated. The retrieval of the above-cloud AOT depends mostly on the aerosol absorption of the light reflected by the cloud. Therefore, it is expected that the retrieved AAOT is less sensitive to the absorbing property of the aerosol than the AOT. The sensitivity of the AAOT to the assumed aerosol properties is shown in Figure 9b and 10b. The uncertainty in the AAOT due to an error in g is similar to the uncertainty in the AOT (<5%). However, the influence of the SSA assumption alone on the AAOT is smaller than the influence on the AOT, with differences of 1.9% and -8.7%. This means that a perturbation of the SSA

primarily impacts the scattering AOT. The largest overestimation of the AAOT (2.7%) is obtained when the assumed aerosol model overestimates g . An underestimation of the SSA and an overestimation of g lead to the largest underestimation of the AAOT (-5.1%).

AAOT rather appears from nowhere at line 350. I think it would benefit from at least a small introduction. Before this, all the focus has been on AOT. Line 373 implies that changing the imaginary part of the refractive index results in a very large perturbation to the AOT retrieval (where does the 39 % actually come from – not obvious from the scatter plots which have points that look like there is a higher difference). You imply that the impact is much smaller on the AAOT but do not really clearly explain why. I think I have worked it out but it is not immediately apparent from the text so I suggest a little rewrite here.

The retrieval is mainly sensitive to the AAOT because it detects the attenuation of the light reflected by the clouds due to the aerosol absorption. Therefore, as the SSA change, the error is expected to primarily affect the scattering AOT. This is why the AOT is more sensitive to the SSA assumption than the AAOT. In section 3c, we added the sentences:

The retrieval of the above-cloud AOT depends mostly on the aerosol absorption of the light reflected by the cloud. Therefore, it is expected that the retrieved AAOT is less sensitive to the absorbing property of the aerosol than the AOT.

This means that a perturbation of the SSA primarily impacts the scattering AOT.

In Section 2a, the following sentence has been added in order to introduce the AAOT:

This attenuation is mainly due to the absorption from the aerosol layer, which means that it is primarily correlated to the Absorption AOT (AAOT).

Are you sure that your uncertainty terms in equation 4 are independent? I would think not given how (I think) the size distribution and refractive indices have been derived. Moreover, even if they are independent, this is only the uncertainty due to the aerosol model. Uncertainty in the water vapour correction (and cloud top height) will also inflate the uncertainty in the final retrievals. Are these combined anywhere?

This part has been removed from the paper. Instead, we have analysed the impact of a perturbation of the SSA and g , both independently and combined. Contrary to the uncertainty on the atmospheric correction, the uncertainties on the aerosol model depends on the assumptions made in the retrieval algorithm. The following sentences have been added at the end of Section 2d:

It is important to realise that the uncertainties that we quantify here are structural and parametric uncertainties related to assumptions made in the retrieval algorithm. When using a fixed aerosol model, no account is made for natural variability in the aerosol optical parameters and the associated uncertainty; this is dealt with in the uncertainty analysis that follows.

In line 382 you state the aerosol model uncertainty as 31 %. It's not immediately obvious how this is consistent with your earlier statement that the uncertainty from the imaginary part of the refractive index can reach 39 % so how do you arrive at this number (could be due to absolute values but it would be nice to be clear)?

This part of the manuscript has been removed and we do not use the absolute average difference anymore. The uncertainty on the retrieved property is defined as the difference between the mean property retrieved with the CLARIFY model and with the mean property retrieved with the modified aerosol model.

I find the evaluation of the retrievals a little lacking. The comparisons to AERONET and MODIS in section 3(a) are very qualitative. It seems obvious to at least include the equivalent MODIS retrievals in figure 12 simply to give some idea of the quantitative consistency between these and the SEVIRI estimates even if it is not clear which, if either, estimate is correct. This should still leave plenty of scope to enlarge on these comparisons in the planned companion paper.

In the region of analysis in Section 4, there is a gap between the two MODIS overpasses in the morning of 05 September and in the afternoon of 06 September. In this area, there is a strong gradient of AOT and it is preferable to compare collocated observations.

Instead of the operational MODIS cloud products, the new Figure 6 in the manuscript shows the maps of the equivalent MODIS aerosol and cloud properties from the MOD06ACAERO retrieval. A short description of these results and how they compare to the SEVIRI products has been added to Section 3a:

As a comparison, Figure 6 shows the equivalent aerosol and cloud properties retrieved from MODIS-Terra with the MOD06ACAERO algorithm (Meyer et al., 2015) for the 10:00 and 11:30 UTC overpasses. The MODIS above-cloud AOT pixels associated with an uncertainty larger than 100% have been removed. A good spatial agreement is observed between the two satellites products. The above-cloud AOT from MODIS is also 1.0 on average close to the coast. On average over the map, the MODIS above-cloud AOT is larger by 0.05 compared to SEVIRI. Considering that MODIS is less sensitive to the atmospheric absorption and that the two algorithms are based on the same principle, the small differences observed between the two above-cloud AOT tend to validate the atmospheric correction applied on the SEVIRI measurements for that case. There is a good consistency between the MODIS and the SEVIRI COT. Finally, the CER retrieved with the MOD06ACAERO algorithm is larger by 2.2 μm compared to the SEVIRI CER. This almost systematic difference is mainly due to differences in the satellite instruments, and especially, the difference in the channels used for the retrieval (Platnick, 2000).

I think the linear trends in Figure 12 add nothing. I'd much prefer to see the individual standard deviations and perhaps even the estimated uncertainty (which are not the same).

The linear trends have been removed from the figure. In the new version of the manuscript, the stability of the retrieval is also assessed at pixel level by evaluating the variability of the above-cloud AOT between continuous observations. The following analysis has been added at the end of Section 4:

The performance of the algorithm is further assessed by evaluating the stability of the retrieved above-cloud AOT at pixel level. As noted by Chang and Christopher (2016), in this region over these scales, aerosols are expected to have a limited temporal variability and the variation of the above-cloud AOT is expected to be small between $t=0$ and $t\pm 15$ minutes. The differences

between the AOT retrieved at $t=0$ and the running mean estimated between $t-15$ and $t+15$ minutes have been calculated at pixel level for observations between 09:00-15:00 UTC, removing measurements within the glory backscattering region. Figure 14 shows the histogram of the AOT differences calculated over a 12-day period (01 to 12 September 2017). The differences follow a normal distribution centred around 0.0 with a standard deviation of 0.1. This short-term variability can be attributed to several sources of uncertainties, such as the total amount of water vapour, its vertical distribution, the retrieved cloud top height and the numerical fitting procedure. This analysis indicates that the retrieval of the above-cloud AOT remains relatively stable, with an observed variability of ± 0.1 between consecutive observations.

Technical Corrections:

At some point early in the manuscript please identify the wavelength(s?) of the COT and AOT retrievals.

Optical thicknesses are given at $0.55\mu\text{m}$. This information is now mentioned in Section 3a:

Throughout this paper, the radiances R refer to the normalized quantity as defined by Herman et al. (2005) and the optical thicknesses (i.e. AOT, COT) are given at $0.55\mu\text{m}$.

Line 48: You've been talking about effect but here you mention forcing. They are not the same. 'of up to'

This sentence has been corrected:

Positive instantaneous DRE of up to $+130\text{W m}^{-2}$ has been observed by satellite instruments over the SEAO (De Graaf et al., 2012; Peers et al., 2015).

Line 59: Here I think you are talking about the aerosol indirect effect. It would good to say this explicitly for consistency with the next sentence.

This sentence has been modified:

Biomass burning particles may also have indirect effects through their interactions with cloud droplets, leading to a modification of the microphysics of the cloud, its lifetime and precipitations (Twomey, 1974; Rosenfeld, 2000).

Line 70: Not sure why 'Aerosols Above Clouds' is capitalised.

Line 86: '...cloud cover over the SEAO has an...'

Line 124: I appreciate the terms may have been defined elsewhere but I think it would be good to explicitly give the definition here.

Line 129: follows

These corrections have been applied.

Line 132: actually from figure 1 there does seem to be some dependence on COT.

This sentence has been modified:

For AOT = 0, the radiance ratio is around 1 and weakly depends on the COT.

Line 143: ‘increases the SWIR’. Actually you do not explicitly define NIR and SWIR in terms of wavelength range. This would be helpful. Or lose the terms entirely and just use the wavelengths.

We chose to refer to the SEVIRI band as visible, NIR and SWIR channel in order to easily compare with other satellite instruments such as MODIS. In the manuscript, the following sentences have been modified:

The SEVIRI instrument, aboard the MSG satellite (Aminou et al., 1997), has channels centred at 0.64, in the visible, and at 0.81 μ m, in the NIR.

As in the Nakajima and King technique (1990), the sensitivity of the retrieval to the CER is brought by the Short-Wave Infra-Red (SWIR) channel of SEVIRI, centred at 1.64 μ m.

Line 166: please explain ‘two-way transmittance’ – from where to where? Why is the two-way transmittance important?

The following information has been added to the manuscript:

(i.e. from the top of the atmosphere to the cloud top and from the cloud top to the top of the atmosphere)

For sake of simplicity, the two-way transmittances will be referred to as transmittances.

Line 228-233: Not really enough detail on ‘weighting’. Someone would struggle to replicate what you have done from this info alone.

The explanation about the weighting of the fit has been rephrased:

In order to obtain the most suitable aerosol optical parameters for the retrieval, it is important to accurately fit the PCASP measurements where the aerosols contribute the most to the SEVIRI signal. Each bin of the PCASP has been assigned a weight for the fit of the bimodal distribution. The weights have been calculated in a similar way to Haywood et al. (2003), which means that they are proportional to the contribution of each bin to the total aerosol extinction in the 0.6 μ m band. The bins corresponding to the 0.15 to 0.25 μ m radius range contribute to about 77% of the extinction. Consequently, these bins have been assigned appropriate larger weights during the fitting process of the size distribution.

Line 255: For the uninitiated it might be useful to say where SAFARI was.

It is now mentioned that the SAFARI and the DABEX measurements were performed over the SEAO.

Line 309: ‘typically observed in this region’ – as shown by who exactly?

We have added the reference to Szczodrak et al. (2001).

The cloud properties retrieved are within the range of values typically observed for marine stratocumulus (Szczodrak et al., 2001) with more than 90 % of the COT lower than 25 and 99 % of the CER between 4 and 20 μm .

Szczodrak, M., Austin, P. H. and Krummel, P. B.: Variability of Optical Depth and Effective Radius in Marine Stratocumulus Clouds, *J. Atmos. Sci.*, 58(19), 2912–2926, doi:10.1175/1520-0469(2001)058<2912:VOODAE>2.0.CO;2, 2001.

Line 322: Can you provide a reference for this statement please.

This sentence has been replaced by:

These errors are likely upper estimates because forecast errors in specific humidity are unlikely to reach these values owing to the extensive assimilation of satellite data and sonde profiles by the data assimilation process used in the Met Office forecast model as previously mentioned.

Line 473-474: This isn't immediately obvious to me. Can you clarify? Obviously you could use a different aerosol model in the LUT but this wouldn't be 'easy'.

In the case where the retrieved AAOT does not depend on the aerosol properties assumed for the retrieval, the AOT retrieved by SEVIRI could be converted from the aerosol model used for the retrieval to another aerosol model using their SSA. To emphasise the importance of the SSA assumption, this sentence has been replaced by the following text in the conclusion:

This uncertainty is led by the sensitivity of the retrieval to the SSA. Because the method relies on the impact of the aerosol absorption on the light reflected by the clouds, the perturbation of the SSA has primarily an impact on the scattering contribution of the AOT. Therefore, a better accuracy is obtained on the retrieved AAOT, with biases generally lower than 17% before 15:00 UTC. After that time, an increase of the uncertainty on both the AOT and the AAOT has been observed, and users are advised to be careful when using the late afternoon aerosol product. For any satellite retrievals based on the colour-ratio technique, aerosol properties, including the SSA, have to be assumed and the same order of magnitude can be expected on the sensitivity of their AOT. This analysis highlights the importance of a suitable constrain on the SSA.

Figure 5(b): You have lost the latitude labels

Figure 7-11: y-axes labels. Suggest adding 1-1 lines.

Figure 12: Add time basis (e.g. UTC).

These corrections have been applied.

1
2 **Observation of absorbing aerosols above clouds over the South-**
3 **East Atlantic Ocean from the geostationary satellite SEVIRI**
4 **Part 1: Method description and sensitivity**

5
6 *Fanny Peers¹, Peter Francis², Cathryn Fox², Steven J. Abel², Kate Szpek², Michael I.*
7 *Cotterell^{1,2}, Nicholas W. Davies^{1,2}, Justin M. Langridge², Kerry G. Meyer³, Steven E.*
8 *Platnick³, Jim M. Haywood^{1,2}*

9
10 (1) College of Engineering, Mathematics, and Physical Sciences, University of Exeter, Exeter, UK
11 (2) Met Office, Exeter, UK
12 (3) NASA Goddard Space Flight Center, Greenbelt, Maryland, USA
13

14 **Abstract**

15
16 High temporal resolution observations from satellites have a great potential for studying the
17 impact of biomass burning aerosols and clouds over the South East Atlantic Ocean (SEAO).
18 This paper presents a method developed to retrieve simultaneously aerosol and cloud properties
19 in aerosol above cloud conditions from the geostationary instrument Meteosat Second
20 Generation/Spinning Enhanced Visible and Infrared Imager (MSG/SEVIRI). The above-cloud
21 Aerosol Optical Thickness (AOT), the Cloud Optical Thickness (COT) and the Cloud droplet
22 Effective Radius (CER) are derived from the spectral contrast and the magnitude of the signal
23 measured in three channels in the visible to shortwave infrared region. The impact of the
24 absorption from atmospheric gases on the satellite signal is corrected by applying
25 transmittances calculated using the water vapour profiles from a Met Office forecast model.
26 The sensitivity analysis shows that a 10% error on the humidity profile leads to an 18.5% bias
27 on the above-cloud AOT, which highlights the importance of an accurate atmospheric
28 correction scheme. *In situ* measurements from the CLARIFY-2017 airborne field campaign are
29 used to constrain the aerosol size distribution and refractive index that is assumed for the
30 aforementioned retrieval algorithm. The sensitivities in the retrieved AOT, COT and CER to
31 the aerosol model assumptions are assessed. Between 09:00-15:00 UTC, an uncertainty of 40%
32 is estimated on the above-cloud AOT, which is dominated by the sensitivity of the retrieval to
33 the single scattering albedo. The absorption AOT is less sensitive to the aerosol assumptions
34 with an uncertainty generally lower than 17% between 09:00-15:00 UTC. Outside of that time
35 range, as the scattering angle decreases, the sensitivity of the AOT and the absorption AOT to
36 the aerosol model increases. The retrieved cloud properties are only weakly sensitive to the
37 aerosol model assumptions throughout the day, with biases lower than 6% on the COT and 3%
38 on the CER. The stability of the retrieval over time is analysed. For observations outside of the
39 backscattering glory region, the time-series of the aerosol and cloud properties are physically
40 consistent, which confirms the ability of the retrieval to monitor the temporal evolution of
41 aerosol above cloud events over the SEAO.
42

Deleted: Although
Deleted: 31.2
Deleted: observed
Deleted: of
Deleted: both
Deleted: is
Deleted: 7%
Deleted: respectively

51 **1. Introduction**

52
53 The South East Atlantic Ocean (SEAO) provides a natural laboratory for analysing the full
54 range of aerosol-cloud-radiation interactions. During the fire season, large amounts of particles
55 from African biomass burning are transported above the semi-permanent deck of stratocumulus
56 covering this oceanic region. As a result, an important contrast is expected in the Direct
57 Radiative Effect (DRE) of aerosols (i.e. the direct impact of aerosol scattering and absorption
58 of radiation). On one hand, the aerosol scattering above the ocean typically increases the local
59 albedo which leads to a negative DRE at the top of the atmosphere. On the other hand, the sign
60 of the DRE above clouds depends on the underlying cloud albedo and the aerosol absorption.
61 Positive instantaneous [DRE of](#) up to $+130\text{W m}^{-2}$ has been observed by satellite instruments
62 over the SEAO (De Graaf et al., 2012; Peers et al., 2015). There are many poorly constrained
63 variables, such as the aerosol and cloud properties, vertical structure of aerosol and clouds
64 (Peers et al., 2016), which result in a large spread in the DRE derived from climate models in
65 this region (Zuidema et al., 2016). In addition, the absorption of radiation by aerosols leads to
66 a modification of the atmospheric stability and consequently on the formation, development
67 and dissipation of clouds, i.e. semi-direct effect. Studies have shown that the overlying African
68 biomass burning aerosols are associated with a cloud thickening (Wilcox, 2010 & 2012). This
69 negative semi-direct effect partly compensates the positive DRE of aerosols above clouds over
70 the SEAO. However, as an aerosol plume moves away from the coast and descends into the
71 boundary layer, the heat due to the aerosol absorption could lead to a reduction of the cloud
72 thickness (Koren et al., 2004). Biomass burning particles may also [have indirect effects through](#)
73 [their interactions](#) with cloud droplets, leading to a modification of the microphysics of the
74 cloud, its lifetime and precipitations (Twomey, 1974; Rosenfeld, 2000). Recent model studies
75 (Gordon et al., 2018; Lu et al., 2018) suggest that the semi-direct and indirect effects of aerosols
76 dominate the DRE over the SEAO, leading to a regional cooling.

Deleted: radiative forcing

77
78 Until recently, there has been a relative dearth of observations of biomass burning above clouds
79 as passive sensor retrievals of aerosol and cloud are generally mutually exclusive. In past
80 studies, biases in cloud properties derived from passive shortwave measurements were
81 expected because the impact of aerosol absorption above clouds was not taken into account in
82 the retrievals (Haywood et al., 2004). Over the last decade, techniques have been developed
83 for the observation of aerosols above clouds. POLDER (Polarization measurements from
84 POLarization and Directionality of the Earth's Reflectances) has been used to detect aerosols
85 above clouds and to characterize the aerosol and the cloud layers by exploiting the sensitivity
86 in polarized measurements (Waquet et al., 2013a & 2013b; Peers et al., 2015). In the case of
87 fine mode absorbing aerosols overlying clouds, the absorption Ångström exponent leads to a
88 greater impact on radiances reflected by the clouds at shorter wavelengths than longer ones
89 (De Graaf et al., 2012; Torres et al., 2012). The “colour-ratio” approach has been applied to
90 OMI (Ozone Monitoring Instrument - Torres et al., 2012) and MODIS (Moderate Resolution
91 Imaging Spectroradiometer - Jethva et al., 2013) to simultaneously retrieve the aerosol and the
92 cloud optical thicknesses over the SEAO. Using a similar technique, the MODIS retrieval
93 developed by Meyer et al. (2015) takes advantage of the 6 channels of the instrument from the

Deleted: interact

96 UV to the Short-Wave Infra-Red (SWIR) to characterize not only the aerosol and cloud optical
97 thicknesses, but also the cloud droplet effective radius. For the first time, these studies have
98 provided large-scale observations of aerosols above clouds in the SEAO. However, these
99 approaches have been applied to satellite instruments on polar-orbiting platforms that provide
100 only two observations per day for MODIS (on the Aqua and Terra platforms) and one for OMI
101 and POLDER. The cloud cover over the SEAO [has](#) an important diurnal cycle which modulates
102 the DRE of aerosols during the day (Min and Zhang, 2014). Therefore, the study of the SEAO
103 cloud and above-cloud aerosol optical properties [would benefit from the high](#) temporal
104 resolution observations [provided by geostationary](#) satellite platforms.

Deleted: is subjected to

Deleted: requires higher

Deleted: from

Deleted: than currently available

105
106 Chang and Christopher (2016) have highlighted the ability of SEVIRI (Spinning Enhanced
107 Visible and Infrared Imager) to identify absorbing aerosols above clouds at high temporal
108 resolution. The instrument is on board the geostationary satellite MSG (Meteosat Second
109 Generation) and provides a full-disc observation every 15 minutes, offering a unique
110 opportunity to monitor the evolution of the cloud cover and to track aerosol plumes over the
111 SEAO. The objective of this two-part paper is to demonstrate the potential of this instrument
112 to retrieve simultaneously aerosol and cloud properties in the case of absorbing aerosols above
113 clouds. In this first contribution, we describe the approach used to derive the above-cloud
114 Aerosol Optical Thickness (AOT), the Cloud Optical Thickness (COT) and the Cloud droplet
115 Effective Radius (CER) and discuss the accuracy of the retrievals. The algorithm, as well as
116 the atmospheric correction scheme and the assumed aerosol model, are presented in Section 2.
117 The sensitivities in the retrieved quantities to the water vapour profile and the aerosol property
118 assumptions are assessed in Section 3. The evaluation of the stability of the retrieval is shown
119 in Section 4 and conclusions are drawn in Section 5. In a second companion paper, we will
120 compare our SEVIRI-based retrievals of cloud and aerosol properties with those from MODIS
121 products (Meyer et al., 2015) [more comprehensively](#) and also [compare against in situ](#) aircraft
122 observations from the CLARIFY-2017 field campaign.

123

124 **2. Retrieval method**

125

126 **a. Principle**

127

128 The approach used to retrieve aerosol and cloud properties from satellite spectral radiance
129 measurements relies on the colour-ratio effect (Jethva et al., 2013). The signal backscattered
130 by a liquid cloud is almost spectrally neutral from the UV to the Near Infra-Red (NIR). On the
131 other hand, the absorption from biomass burning aerosols is typically larger at shorter
132 wavelengths. Therefore, the presence of absorbing aerosols above clouds modifies the apparent
133 colour of clouds. This enhancement of the spectral contrast can be detected by any passive
134 remote sensing instrument with two channels with enough separation in the UV/NIR region.
135 The SEVIRI instrument, aboard the MSG satellite (Aminou et al., 1997), has channels centred
136 at 0.64 [in the visible](#), and at 0.81 μm , [in the NIR](#). Figure 1 plots the 0.81 μm radiance ($R_{0.81}$)
137 against the ratio of the 0.64 to 0.81 μm radiances ($R_{0.64}/R_{0.81}$), for absorbing aerosols above
138 clouds over an ocean surface for several aerosol and cloud optical thicknesses. Throughout this

143 paper, the radiances R refer to the normalized quantity as defined by Herman et al. (2005) and
144 the optical thicknesses (i.e. AOT, COT) are given at $0.55\mu\text{m}$. The simulations have been
145 performed with the adding-doubling method (De Haan et al., 1987), considering a viewing
146 geometry of 20° for the solar zenith angle, 50° for the viewing zenith angle and 140° for the
147 relative azimuth. The cloud is located between 0 and 1 km and the aerosol layer is between 2
148 and 3 km. Aerosols have a refractive index of $1.54 - 0.025i$ and the size distribution follows a
149 lognormal with a geometric mean radius of $0.1\mu\text{m}$. The cloud droplets have an effective radius
150 of $10\mu\text{m}$. Rayleigh scattering has been accounted for but the simulations do not include the
151 absorption from atmospheric gases. A Lambertian surface with an albedo of 0.05 is assumed.
152 For AOT = 0, the radiance ratio is around 1 and weakly depends on the COT. As the AOT
153 increases, the radiance at $0.81\mu\text{m}$ as well as the radiance ratio decreases, indicating that the
154 attenuation from the aerosol layer is larger at $0.64\mu\text{m}$. This attenuation is mainly due to the
155 absorption from the aerosol layer, which means that it is primarily correlated to the Absorption
156 AOT (AAOT).

Deleted: (2005).

Deleted: follow

Deleted: is largely invariant as a function of COT.

157
158 As in the Nakajima and King technique (1990), the sensitivity of the retrieval to the CER is
159 brought by the Short-Wave Infra-Red (SWIR) channel of SEVIRI, centred at $1.64\mu\text{m}$. Figure
160 2 shows the radiances at 0.81 and $1.64\mu\text{m}$ for several COT and CER as well as the impact of
161 overlying absorbing aerosols. The simulations without aerosol are plotted in blue and represent
162 the signal typically used by cloud property retrievals that do not include light absorption from
163 overlying aerosols. The orange and red grids are associated with an AOT of 0.5 and 1.5 at
164 $0.55\mu\text{m}$. Compared to the no-aerosol case, these grids are shifted towards the upper left, which
165 means that the presence of aerosols decreases the NIR radiance and increases in the SWIR
166 signal. As highlighted by Haywood et al. (2004), not taking into account the aerosol absorption
167 above clouds leads to low biases in both the COT and the CER. These biases depend on the
168 aerosol loading as well as on the brightness of the underlying cloud.

169
170 Although the aerosol microphysical properties have some influence on the signal measured by
171 satellites, this kind of approach requires us to assume an aerosol model. Fundamentally, the
172 algorithm developed here aims to retrieve the above-cloud AOT, the COT and the CER from the
173 magnitude and the gradient of the radiances measured by SEVIRI at 0.64 , 0.81 and 1.64
174 μm using a basic Look Up Table (LUT) approach and appropriate assumptions about the
175 aerosol model, for the region (Haywood et al., 2003) that have been refined based on
176 measurements from the CLARIFY-2017 observational campaign (Zuidema et al., 2016).

Deleted: .

178 b. Atmospheric correction

179
180 The SEVIRI channels chosen for the retrieval are fairly standard in atmospheric science and
181 have been widely used for aerosol and cloud analysis (e.g. Brindley and Ignatov, 2006;
182 Thieuleux, et al. 2005; Watts et al., 1998). However, the SEVIRI bandwidths are much larger
183 than other state-of-the-art instruments such as MODIS. Hence, SEVIRI radiances are
184 significantly more impacted by the absorption from various atmospheric gases. The spectral
185 response functions for the 0.64 , 0.81 and $1.64\mu\text{m}$ SEVIRI channels are plotted in Figure 3

Deleted: , and hence

Deleted: to a greater degree

192 together with the equivalent MODIS bands. The main absorbing gases in these spectral bands
193 are ozone, water vapour, methane and carbon dioxide; gases which are typically produced and
194 transported within biomass burning plumes (Browell et al., 1996; Koppmann et al., 2005). The
195 contributions of each gas to the atmospheric absorption are also shown in Figure 3 and the two-
196 way transmittances (i.e. from the top of the atmosphere to the cloud top and from the cloud top
197 to the top of the atmosphere) weighted by the spectral response function have been calculated.
198 For sake of simplicity, the two-way transmittances will be referred to as transmittances.

199 Although the MODIS bandwidths are narrower than the SEVIRI ones, the weighted
200 transmittances are similar for the 0.64 and 1.64 μm channels. In the NIR, the MODIS central
201 wavelength (0.86 μm) is slightly larger than for SEVIRI (0.81 μm) and the spectral band is
202 only weakly impacted by the humidity, with a weighted transmittance of 0.989. Within the
203 SEVIRI band, water vapour absorption is much higher, with a transmittance of 0.931. As a
204 result, humidity has an impact on the spectral contrast between the VIS and the NIR, and
205 therefore, on the above-cloud AOT retrieval. The atmospheric correction, especially for the
206 water vapour, is essential to accurately retrieve the aerosol and cloud properties from SEVIRI.

207

208 In order to correct the SEVIRI measurements for atmospheric absorption, the transmittances
209 $T_{\text{atm},\lambda}$ are calculated for each spectral band λ from the cloud top height to the top of the
210 atmosphere using the fast-radiative transfer model RTTOV (Matricardi et al., 2004; Hocking
211 et al., 2014). The cloud top height is derived from the Met Office cloud property algorithm
212 which uses the 10.8, 12.0 and 13.4 μm channels of SEVIRI (Francis et al., 2008, Hamann et
213 al., 2014). Water vapour profiles come from the operational forecast configuration of the global
214 Met Office Unified Model (Brown et al., 2012). This forecast is assimilated according to the
215 scheme described by Clayton et al. (2013) that uses humidity data from various sources,
216 including radiosondes and remote sensing sounding data from many meteorological satellites.
217 The forecast is run every 6 hours and the humidity profile used for the atmospheric correction
218 comes from the latest time-appropriate forecast field available. The profiles of the remaining
219 gases - including ozone, carbon dioxide and methane - are those implicitly assumed by the
220 RTTOV calculations (Matricardi, 2008). The radiance measured by SEVIRI $R_{\text{atm},\lambda}$ is finally
221 corrected using:

$$R_{\text{atm},\lambda} = T_{\text{atm},\lambda} R_{\lambda} \quad (1)$$

222 where R_{λ} is the radiance corrected from the gaseous absorption.

223

224 c. Aerosol model

225

226 The choice of the aerosol microphysical properties to use for the retrieval is similar to that of
227 Haywood et al (2003), but based on more comprehensive *in situ* measurements acquired during
228 the CLARIFY-2017 field campaign. The Facility for Airborne Atmospheric Measurements
229 (FAAM) BAe 146 aircraft was deployed in August-September 2017 operating from Ascension
230 Island, with a main objective of studying biomass burning aerosol interactions with both
231 radiation and clouds over the SEAO. This analysis focuses on flight C050, performed on 04
232 September, 2017. A profile descent from 7.3 to 1.9 km altitude was performed in order to
233 sample the aerosol layer above clouds.

Deleted: and

Deleted: one

Deleted: based on

237

238 The aerosol dry extinction and absorption were measured with the EXSCALABAR instrument
239 (EXtinction, SCattering and Absorption of Light for AirBorne Aerosol Research), which
240 consists of a series of cavity ring-down and photoacoustic absorption cells operating at
241 different wavelengths (Davies et al., 2018). From these *in situ* measurements, the Single
242 Scattering Albedo (SSA) has been calculated at the instrument wavelengths of 405 and ~~658~~
243 nm. The uncertainty in SSA calculations are related to the corresponding uncertainties in the
244 extinction and absorption coefficients measured by EXSCALABAR. This error analysis has
245 been performed previously and the reader is directed to Davies et al. (2019). Briefly, the
246 measured extinction has an accuracy of ~2%, and we use a 2% extinction uncertainty in the
247 analysis here. The errors in absorption measurements using photoacoustic spectroscopy depend
248 on uncertainties in the ozone calibration, microphone pressure dependence and the background
249 response from laser scattering/absorption on the windows of the photoacoustic cell. We have
250 shown in recent publications that our calibration uncertainties are ~5% (Cotterell et al. 2019;
251 Davies et al. 2018), and the uncertainty in the pressure-dependent microphone response is 1.2%
252 (Davies et al. 2019). The background response from laser-window interactions is from 0.27
253 and 0.54 Mm⁻¹. Thus, the total absorption uncertainty, propagating all the above uncertainties,
254 is absorption-dependent and ranges from 29.0 – 55.0 % (dependent on PAS measurement
255 wavelength) at 1 Mm⁻¹ and 8.1 % at 100 Mm⁻¹ (independent of PAS measurement wavelength).
256 We propagated these total measurement uncertainties for both extinction and absorption
257 measurements to derive the standard deviation σ in our calculated SSA values. We find that
258 the mean SSA uncertainties are 0.013 and 0.018 at the measurement wavelengths of 405 and
259 658 nm respectively.

Deleted: 660 nm.

260

261 The aerosol size distribution was characterized between 0.05 and 1.50 μm radius using a wing-
262 mounted Passive Cavity Aerosol Spectrometer Probe (PCASP). Before and after the campaign,
263 the bin sizes of the PCASP were calibrated using aerosolized diethylhexyl sebacate and
264 polystyrene latex of known size and refractive index (Rosenberg et al., 2012). Further Mie-
265 scattering theory based calculations are performed in order to determine the bin sizes at the
266 refractive index of the biomass burning aerosol sample. Partial evaporation of water is expected
267 in the PCASP due to the heating of the probe, which may decrease the aerosol size. However,
268 the sonde dropped during the flight indicates an average relative humidity above clouds of
269 29.2% with a maximum of 38.6%. According to Magi and Hobbs (2003), the light scattering
270 coefficient of an aged African biomass burning plume only increases by a factor of 1.01 for a
271 relative humidity of 40%. For this reason, the impact of humidity on the PCASP and
272 EXSCALABAR measurements is neglected. Three sources of errors have been taken into
273 account on the PCASP measurements: the error on the bin concentration is calculated
274 according to Poisson counting statistics, the sample flow rate error is assumed to be 10% and
275 a bin edge calibration error of half a bin has been considered.

Deleted: of hydration

276

277 The aerosol properties needed for the SEVIRI retrieval include the size distribution and the
278 complex refractive index. The normalized number size distribution ($dN/d\ln r$) is commonly
279 represented by a combination of lognormal modes:

Deleted: are

$$\frac{dN}{d \ln r} = \sum_i \frac{N_i}{\sqrt{2\pi}} \frac{1}{\ln \sigma_i} \exp \left[\frac{-(\ln r_i - \ln r)^2}{2(\ln \sigma_i)^2} \right] \quad (2)$$

283 where N_i , r_i and σ_i are the number fraction, the geometric mean radii and the standard deviation
 284 of the mode i , respectively. As in most remote sensing applications, it has been chosen to
 285 represent the particle size distribution for the aerosol during CLARIFY-2017 with a fine and a
 286 coarse mode contributions. The aerosol [optical properties are calculated using the Mie theory,](#)
 287 [as the spherical approximation is expected to be valid for biomass burning particles from one](#)
 288 [hour after being released in the atmosphere \(Martins et al., 1998\). The aerosol model is selected](#)
 289 [by iteratively adjusting the refractive index and fitting the PCASP measurements \(Fig. 4a\) until](#)
 290 [the aerosol model matches the SSA from EXSCALABAR \(Fig. 4b\). In order to obtain the most](#)
 291 [suitable aerosol optical parameters for the retrieval, it is important to accurately fit the PCASP](#)
 292 [measurements where the aerosols contribute the most to the SEVIRI signal. Each bin of the](#)
 293 [PCASP has been assigned a weight for the fit of the bimodal distribution. The weights have](#)
 294 [been calculated in a similar way to Haywood et al. \(2003\), which means that they are](#)
 295 [proportional to the contribution of each bin to the total aerosol extinction in the 0.6 \$\mu\text{m}\$ band.](#)
 296 The bins corresponding to the 0.15 to 0.25 μm radius range contribute to about 77% of the
 297 extinction. Consequently, these bins have been assigned appropriate larger weights during the
 298 fitting process of the size distribution. Due to the small fraction of coarse mode aerosols,
 299 the standard deviation of this mode σ_{coarse} could not be reliably fitted and has been set to a value
 300 of 2.23, which is within the same order of magnitude than the one assumed for absorbing
 301 aerosol (~ 2.12) in the MODIS Dark Target operational algorithm (Levy et al., 2009).

302
 303 The aerosol model that best represents the PCASP and EXSCALABAR measurements is
 304 shown in blue on Figures 4a and 4b. A refractive index of 1.51-0.029i has been obtained,
 305 associated with an SSA of 0.85 at 0.55 μm which is within the range of SSA measured [over](#)
 306 [the SEAO](#) during the SAFARI and the DABEX campaigns (Johnson et al., 2008) and on the
 307 upper end of the values from Ascension Island reported by Zuidema et al. (2018). Regarding
 308 the refractive index, it should be noted that the SSA is not very sensitive to the real part
 309 suggesting that the value of 1.51 is not particularly well constrained. However, a real part of
 310 1.51 is consistent with the AERONET retrievals for African biomass burning particles (Sayer
 311 et al., 2014) and is adopted here. The best-fit size distribution is characterised by $[r_{fine}, \sigma_{fine},$
 312 $N_{fine}; r_{coarse}, \sigma_{coarse}, N_{coarse}] = [0.12\mu\text{m}, 1.42, 0.9996; 0.62\mu\text{m}, 2.23, 0.0004]$. By way of
 313 comparison, the 3-mode lognormal distribution obtained for aged biomass burning aerosols
 314 during the SAFARI 2000 campaign (Haywood et al., 2003), defined by $[r_1, \sigma_1, N_1; r_2, \sigma_2, N_2;$
 315 $r_3, \sigma_3, N_3] = [0.12\mu\text{m}, 1.30, 0.996; 0.26\mu\text{m}, 1.50, 0.0033; 0.80\mu\text{m}, 1.90, 0.0007]$, is plotted in
 316 orange on Figure 4a. The radius associated with the first mode is consistent with the CLARIFY-
 317 2017 model. The absence of the second fine mode in this study is compensated by a larger
 318 standard deviation for the fine mode. Finally, the radius of the CLARIFY-2017 coarse mode is
 319 slightly smaller than the SAFARI-2000 one but the coarse mode fractions of the two models
 320 are close to each other. The uncertainties on the aerosol properties have been estimated using
 321 the errors on the PCASP and EXSCALABAR measurements. The uncertainty on the imaginary
 322 part of the refractive index is 0.02 for the real part and 0.004 for the imaginary part. For the

Deleted: and resulting optical parameters are

Deleted: simultaneously

Deleted: and

Deleted: 4b) using Mie theory.

Deleted: has been weighted in order to accurately represent the size range where the SEVIRI retrieval is the most sensitive. The contribution of each PCASP bin to the extinction has

Deleted: (2003).

Deleted: one but the coarse mode fractions of the two models are close

334 [size distribution, the uncertainty is 0.016 \$\mu\$ m, 0.09 and 0.00045 for radius, the standard](#)
335 [deviation and the number fraction of the fine mode respectively.](#)

336

337 **d. Algorithm**

338

339 The algorithm relies on the comparison of the corrected SEVIRI signal at 0.64, 0.81 and 1.64
340 μ m with precomputed radiances. The simulations have been performed using an adding-
341 doubling radiative transfer code (De Haan et al., 1987). The surface is assumed to be
342 Lambertian with an albedo of 0.05 at all wavelengths which is typical of the sea-surface albedo
343 under diffuse radiation conditions. The aerosol and cloud properties assumed for the LUT are
344 summarized in Table 1. The truncation of the cloud droplet phase function has been done using
345 the delta-M method (Wiscombe, 1977) and the TMS correction (Nakajima and Tanaka, 1988)
346 has been applied. The cloud layer is [assumed to be](#) located between 0 and 1 km and the aerosol
347 layer between 2 and 3 km. The sensitivity of the algorithm to the altitudes of the aerosol and
348 cloud layers is expected to be negligible due to the small contribution of the Rayleigh scattering
349 to the signal at the SEVIRI wavelengths. [We have evaluated the error due to the fixed aerosol](#)
350 [and cloud altitudes to be lower than 2.5% on the AOT and 0.3% on the cloud properties.](#) The
351 cloud droplets [are assumed to](#) follow a gamma law distribution characterised by an effective
352 variance of 0.06. When the cloud is optically thin and/or the cloud droplets are too small, it is
353 not possible to separate the contribution to the optical signal arising from aerosols from that of
354 clouds. Therefore, the minimum values for the CER and the COT in the LUT are 4 μ m and 3,
355 respectively. This also justifies the assumption of a relatively simple sea-surface reflectance
356 parameterisation as, at COTs exceeding 3, the sea-surface has little impact on the upwelling
357 radiances above clouds. Clouds associated with lower COT and/or CER are rejected. The
358 aerosol model corresponds to the CLARIFY-2017 model mentioned above, assuming the same
359 refractive index at the 3 SEVIRI wavelengths.

360

361 The retrieval of the above-cloud AOT, COT and CER is performed simultaneously. The result
362 corresponds to the parameters that minimise the difference ε between the simulated radiances
363 R_{sim} and the corrected satellite signal R_λ :

$$\varepsilon = \sum_{\lambda} \left(\frac{R_{\lambda} - R_{sim,\lambda}}{R_{\lambda}} \right)^2 \quad (3)$$

364 When the simulated signal is not close enough to the satellite measurements (i.e. $\varepsilon > 0.0006$),
365 the result is rejected. The retrieval of the above-cloud AOT is highly uncertain at the cloud
366 edges and for inhomogeneous clouds. In order to remove these results, the products are
367 aggregated onto a $0.1 \times 0.1^\circ$ grid and the standard deviation of the AOT and the CER are
368 calculated. Note that each grid cell represents [approximately](#) 12 SEVIRI [pixels](#). The
369 inhomogeneity parameter ρ is defined by the ratio of the standard deviation of a parameter to
370 the average value of this parameter. The results corresponding to a standard deviation of the
371 AOT larger than 0.7 and/or $\rho_{CER} > 0.2$ as well as grid cells associated with less than 9 successful
372 retrievals are rejected.

373

Deleted: of

Deleted: around

Deleted: observations

377 [It is important to realise that the uncertainties that we quantify here are structural and](#)
378 [parametric uncertainties related to assumptions made in the retrieval algorithm. When using a](#)
379 [fixed aerosol model, no account is made for natural variability in the aerosol optical parameters](#)
380 [and the associated uncertainty; this is dealt with in the uncertainty analysis that follows.](#)
381

382 **3. Results and uncertainty analysis**

383 **a. Case study**

386 The algorithm has been applied to an event of biomass burning aerosols above clouds captured
387 by SEVIRI on 28 August 2017 at 10:12 UTC. The RGB composite, the retrieved above-cloud
388 AOT, COT and CER over the SEAO region are shown in Figure 5. The largest AOT are
389 observed off the coast of Angola, with a local average value of 1.0 and a maximum of 1.6 at
390 [0.55 \$\mu\text{m}\$](#) . The AERONET site of Lubango (14.96 °S - 13.45 °E) measured an average AOT of
391 0.75 that day with an Ångström exponent of 1.83, indicating the expected domination of fine
392 mode biomass burning aerosols. A gradient of AOT is observed towards the south-west, as we
393 move away from the source as might be expected from a pre-campaign analysis of satellite
394 retrievals (Zuidema et al., 2016). Absorbing aerosols above clouds are also detected in the
395 north-west part of the region. Around Ascension Island (7.98 °S - 14.42 °W), the above-cloud
396 AOT from SEVIRI is around 0.37 while the AERONET site indicates a value of 0.48 associated
397 with an Ångström exponent of 1.271. This suggests that coarse mode aerosols, such as sea salt
398 within the boundary layer but generally below cloud, are contributing to the total column
399 aerosol load. The cloud properties retrieved are within the range of values typically observed
400 [for marine stratocumulus \(Szczodrak et al., 2001\)](#) with more than 90 % of the COT lower than
401 25 and 99 % of the CER between 4 and 20 μm . [As a comparison, Figure 6 shows the equivalent](#)
402 [aerosol and cloud properties retrieved from MODIS-Terra with the MOD06ACAERO](#)
403 [algorithm \(Meyer et al., 2015\) for the 10:00 and 11:30 UTC overpasses. The MODIS above-](#)
404 [cloud AOT pixels associated with an uncertainty larger than 100% have been removed. A good](#)
405 [spatial agreement is observed between the two satellites products. The above-cloud AOT from](#)
406 [MODIS is also 1.0 on average close to the coast. On average over the area, the MODIS above-](#)
407 [cloud AOT is larger by 0.05 compared to SEVIRI. Considering that MODIS is less sensitive](#)
408 [to the atmospheric absorption and that the two algorithms are based on the same principle, the](#)
409 [small differences observed between the two above-cloud AOT tend to validate the atmospheric](#)
410 [correction applied on the SEVIRI measurements for that case. There is a good consistency](#)
411 [between the MODIS and the SEVIRI COT. Finally, the CER retrieved with the](#)
412 [MOD06ACAERO algorithm is larger by 2.2 \$\mu\text{m}\$ compared to the SEVIRI CER. This almost](#)
413 [systematic difference is mainly due to differences in the satellite instruments, and especially,](#)
414 [the difference in the channels used for the retrieval \(Platnick, 2000\). A fully statistical analysis](#)
415 [against the MODIS algorithm, and against airborne remote sensing and *in situ* measurements](#)
416 [will be presented in a companion paper.](#)
417

Deleted: the

Deleted: 550 nm

Deleted: in this region

Deleted: obtained

Deleted: cloud properties and the standard MODIS operational

Deleted: from the Terra overpasses at 10:00 and 11:30 UTC (Fig. 6). Further comparisons

426
427
428
429
430
431
432
433
434
435
436
437
438
439
440
441
442
443
444
445
446
447
448
449
450
451
452
453
454
455
456
457
458
459
460
461
462
463
464
465
466
467
468

b. Atmospheric correction

The atmospheric transmittances above clouds used to correct the SEVIRI measurements from the gas absorption are calculated based on [forecast](#) water vapour profiles. In order to assess the sensitivity of the retrieval to the atmospheric correction, new transmittances have been calculated for the event studied here, modifying the specific humidity by +/-10%. The aerosol and cloud properties retrieved with the modified atmospheric corrections are aggregated on a $0.1 \times 0.1^\circ$ grid. Figure 7 compares the retrieved aerosol and cloud properties from SEVIRI-measured radiances using the original [specific humidity](#) forecast with the perturbed [specific humidity](#) (+10% in orange and -10% in blue). The uncertainty on the water vapour content impacts mainly the retrieval of the above-cloud AOT, and then the COT, because of its effect on the radiance ratio. A +10%/-10% bias on the humidity leads to an overestimation/underestimation of the AOT and COT respectively. On average, errors of 18.5%, 5.5% and 2.3% have been calculated for the AOT, COT and CER respectively, based on biases of 10% in the [specific humidity](#) forecast. These errors are likely upper estimates because forecast errors in specific humidity are unlikely to reach these values [owing to the extensive assimilation of satellite data and sonde profiles by the data assimilation process used in the Met Office forecast model](#) as previously mentioned. However, the differences between forecast model specific humidities and those of simple standard atmosphere climatological values (e.g. those of McClatchey et al., 1972) frequently exceed 10%, indicating that accurate retrievals of aerosol and cloud need synergistic retrievals or data assimilated forecasts of specific humidity.

c. Aerosol model

The LUT used for the SEVIRI retrieval uses an assumed aerosol model based on *in situ* measurements from CLARIFY-2017. However, the absorption property and the size of biomass burning particles are expected to vary during the fire season and across the SEAO (e.g. Eck et al., 2003). Here, we analyse the impact of the aerosol assumptions on the retrieved aerosol and cloud properties.

[In order to create a range of aerosol optical properties, a thousand aerosol models have been processed using the Mie theory. The radius and the standard deviation of the fine mode, and the real and imaginary part of the refractive index of the models are random values following a normal distribution. Their mean corresponds to the CLARIFY model values provided in Table 1, with standard deviations of \$0.01\mu\text{m}\$ and \$0.1\$ for the radius and the standard deviation of the fine mode, \$0.02\$ for the real part of the refractive index and \$0.008\$ for the imaginary part. Figure 8a and 8b show the histograms of the simulated SSA and asymmetry factor \$g\$ at \$0.55\mu\text{m}\$ in orange. As a comparison, histograms of the AERONET SSA and \$g\$ are plotted in blue. The data corresponds to the AERONET level 2.0 retrievals for August-September, from 1997 to 2018 and for inland sites of Southern Africa \(\$10^\circ\text{S}\$ – \$35^\circ\text{S}\$, \$10^\circ\text{E}\$ – \$40^\circ\text{E}\$ \). Only data associated with an Ångström exponent larger than 1.0 have been used in order to remove measurements dominated by coarse mode particles \(such as dust and sea salt\) that are less likely to be observed](#)

Deleted: forecasted

Deleted: %, which can be considered as an upper limit for the error in the forecast model.

Deleted: RH

Deleted: RH

Deleted: RH

Deleted: %

Moved down [1]: After aggregating the data on a $0.1 \times 0.1^\circ$ grid, the AOT as well as the Absorption AOT (AAOT), the COT and the CER are compared against those obtained with the standard CLARIFY-2017 aerosol model.

Deleted: New LUTs have been processed, independently modifying each of the following parameters of the CLARIFY-2017 aerosol model: the radius and the standard deviation of the fine mode, the real and the imaginary part of the refractive index. The ranges of the parameter perturbations have been chosen in an attempt to represent the variability of the biomass burning properties over the SEAO. The aerosol properties used for this analysis are summarized in Table 2. The new LUTs have been used to re-process the case study from section 3.a.

490 above clouds in the SEAO. The mean SSA (0.862) and the mean g (0.620) from AERONET
491 are respectively slightly larger and smaller than the CLARIFY model. Small differences
492 between above-cloud and full column aerosol properties could be explained by the contribution
493 of aerosol within the boundary layer, such as pollution, desert dust and sea salt. The dashed
494 lines in Figure 8a and 8b represent the mean +/- the standard deviation of SSA and g. The
495 AERONET standard deviation is 0.023 for the SSA and 0.024 for g while the simulation
496 produces a standard deviation of 0.036 for the SSA and 0.041 for g. The simulated range of
497 both optical properties is larger than the range observed by AERONET. Therefore, the
498 variation of the aerosol microphysical properties used for the simulations is wide enough to
499 cover the range of observed aerosol optical properties.

500
501 From the simulated standard deviation σ of g and SSA, eight aerosol models have been defined
502 and their properties are summarized in Table 2. The first four are used to test the sensitivity of
503 the retrieval to g and SSA independently ($[SSA_{\text{CLARIFY}} \pm \sigma_{\text{SSA}}, g_{\text{CLARIFY}}]$ and $[SSA_{\text{CLARIFY}},$
504 $g_{\text{CLARIFY}} \pm \sigma_g]$) and the sensitivity to both parameters will be assessed with the last four
505 ($[SSA_{\text{CLARIFY}} \pm \sigma_{\text{SSA}}, g_{\text{CLARIFY}} \pm \sigma_g]$). New LUTs have been processed with these modified
506 aerosol models and used to re-process the case study from section 3 a. ~~After aggregating the~~
507 ~~data on a $0.1 \times 0.1^\circ$ grid, the AOT as well as the Absorption AOT (AAOT), the COT and the~~
508 ~~CER are compared against those obtained with the standard CLARIFY-2017 aerosol model.~~
509 Results are shown in Figure 9 and 10. For each aerosol and cloud property, a linear relationship
510 is observed between the retrieval using the standard CLARIFY-2017 aerosol model and the
511 modified one. The retrieval of cloud properties (fig. 9c, 9d, 10c and 10d) appears to be weakly
512 sensitive to the assumed aerosol model, with g having a slightly larger impact. On average,
513 differences lower than 4.1% are observed on the COT and lower than 2.4% on the CER. As
514 expected, the choice of the aerosol model has much more influence on the AOT retrieval. The
515 uncertainty on the AOT is dominated by the SSA assumption. When aerosols are more
516 absorbing than the CLARIFY model, the algorithm overestimates the AOT by 25.7%.
517 Conversely, the retrieved AOT is underestimated by 32.6% when aerosols are less absorbing
518 than the CLARIFY model. The impact of g alone on the retrieved AOT is far less significant
519 and lower than 4.3%. Figure 9a, which shows the impact of a perturbation on both the SSA and
520 g, confirms that the SSA is the parameter with the strongest influence on the AOT retrieval.
521 The largest overestimation (27.5%) is observed when both the SSA and g are overestimated
522 (fig. 10a), while the largest underestimation (-33.3%) is obtained when the SSA is
523 underestimated and g is overestimated. The retrieval of the above-cloud AOT depends mostly
524 on the aerosol absorption of the light reflected by the cloud. Therefore, it is expected that the
525 retrieved AAOT is less sensitive to the absorbing property of the aerosol than the AOT. The
526 sensitivity of the AAOT to the assumed aerosol properties is shown in Figure 9b and 10b. The
527 uncertainty in the AAOT due to an error in g is similar to the uncertainty in the AOT (<5%).
528 However, the influence of the SSA assumption alone on the AAOT is smaller than the influence
529 on the AOT, with differences of 1.9% and -8.7%. This means that a perturbation of the SSA
530 primarily impacts the scattering AOT. The largest overestimation of the AAOT (2.7%) is
531 obtained when the assumed aerosol model overestimates g. An underestimation of the SSA and
532 an overestimation of g lead to the largest underestimation of the AAOT (-5.1%).

Moved (insertion) [1]

Deleted: Figure 8 and 9 show the impact of a variation of +/- 0.01 μm on the fine mode radius and +/-0.1 on the fine mode standard deviation. For each aerosol and cloud property, a linear relationship is observed between the retrieval using the standard CLARIFY-2017 aerosol model and the modified one. The aerosol size distribution has little influence on the retrieved cloud properties. On average, the modification of the fine mode standard deviation leads to a difference of 2.2% on the COT and 1.0% the CER. The effect associated with a change in the fine mode radius is even lower than 1%. As expected, the above-cloud AOT is more sensitive to the aerosol size distribution used for the inversion and differences up to 11.8% have been observed when the fine mode standard deviation is decreased by 0.1. However, the retrieval of the AOT is based on the detection of the aerosol absorption of the light reflected by the clouds. Therefore, the impact of an error on the aerosol size distribution on the AAOT retrieval is reduced to 5.4% for the standard deviation and 1.4% for the fine mode radius. .

... [1]

553

554 The variation of the solar zenith angle, and therefore, of the satellite observation geometry
555 during the day can impact the sensitivity of the retrieval to the aerosol assumptions. Therefore,
556 the 15-minute SEVIRI observations for the 28 August have been processed using the eight
557 aerosol models described above and compared to the aerosol and cloud properties retrieved
558 with the CLARIFY aerosol model. The difference Δx_i of a product x is defined as:

$$559 \quad \Delta x_i = (x_{\text{CLARIFY}} - x_i) / x_i \times 100\%$$

560 where x_{CLARIFY} and x_i is the mean product x retrieved over the SEVIRI slot with the aerosol
561 CLARIFY model and the modified model i , respectively. Figure 11 shows the time series of
562 Δ AOT (a), Δ AAOT (b), Δ COT (c) and Δ CER (d) obtained with the modified aerosol models.
563 The sensitivity of the retrieved cloud properties to the aerosol model assumptions remains
564 small (lower than 5.6% for the COT and 2.6% for the CER) and dominated by the sensitivity
565 to g . Apart from a small decrease of Δ COT at midday when g is overestimated (solid blue line)
566 and an increase of Δ COT in late afternoon when the SSA is underestimated (solid red line), no
567 significant trend is observed on the cloud property sensitivities. As observed previously, the
568 uncertainty on the AOT is led by the SSA assumption, with the AOT being overestimated
569 (respectively underestimated) when the assumed SSA is overestimated (respectively
570 underestimated). Until 15:00, Δ AOT stays within +/-40%, with the sensitivity to the SSA being
571 slightly larger at midday. Then it increases up to 60% when the SSA is overestimated and g is
572 underestimated (dashed blue line). Similar trends are observed on Δ AAOT, with generally
573 lower values than Δ AOT. An increase of the uncertainty is observed on the AAOT after 15:00,
574 that reaches up to 27% at 16:30. Before 15:00, there is a larger AAOT sensitivity to the SSA
575 around midday (+8.9%/-15.2%), but there is no evident evolution of the sensitivity to g with
576 time. The case that lead to the largest biases on the AAOT is when the SSA is underestimated
577 and g overestimated (dashed green lines), with an underestimation of up to 23%. However, it
578 should be noted that 0% of the AERONET observations used in Figure 8 are associated with
579 an SSA lower than $\text{SSA}_{\text{CLARIFY}} - \sigma_{\text{SSA}}$ and a g larger than $g_{\text{CLARIFY}} - \sigma_g$. Otherwise, the sensitivity
580 of the AAOT to the aerosol property assumptions stays between -16.6 and +9% before 15:00.

581

582 In conclusion, the retrieved AOT is less sensitive to the aerosol property assumption before
583 15:00, with an uncertainty of 40%. This uncertainty is dominated by the sensitivity of the
584 retrieval to the SSA. An overestimation (respectively underestimation) of the AOT is expected
585 when the observed aerosols are more (respectively less) absorbing than the aerosol model
586 assumed for the retrieval. A better accuracy is obtained on the retrieved AAOT, with an
587 uncertainty generally lower than 17 % before 15:00. The sensitivity of the cloud properties to
588 the aerosol model assumption remain small all day long, with an uncertainty of 5.6% on the
589 COT and 2.6% on the CER.

590

591 **4. Assessing the stability of the retrieval**

592

593 One of the major benefits from using SEVIRI is the ability to track both aerosol and cloud
594 events at high temporal resolution. Therefore, it is important to evaluate how consistent the
595 retrieval is over time. For that purpose, two days of continuous observations (i.e. 5th and 6th

596 September 2017) have been analysed and the retrieved properties have been averaged over
597 20°S and 10°S, and 5°E and 15°E, [which correspond to the red square on the maps of Figure](#)
598 [12](#). The above-cloud AOT, COT and CER time series are presented in Figures [13a, b and c](#).
599 The studied area is located next to the coast, where the AOT is typically the highest. The above-
600 cloud AOT is around 0.66 and 0.72 for the 5th and the 6th September, respectively. As expected,
601 the transport of the aerosol plume from east to west is slow, resulting in a small evolution of
602 the above-cloud AOT. On both days, a peak is observed at 12:12pm with an anomaly larger
603 than the AOT variability. [This localised discontinuity in the above-cloud AOT is shown in the](#)
604 [11:42, 12:12 and 12:42 UTC maps for 05 September 2017 of Figure 12](#). The evolution of the
605 cloud properties is slightly more complex. A small decrease is observed on both the COT and
606 CER until 2pm. After 3pm, both properties sharply increase. The clouds are strongly affected
607 by the diurnal cycle and a shoaling of the cloud cover is expected from early morning to late
608 afternoon. As the thinnest clouds vanish, the cloud fraction decreases together with the number
609 of retrievals in the area. This results in a larger contribution of the thickest clouds to the mean
610 value in the late afternoon. As for the above-cloud AOT, large variations of the CER are
611 observed around noon. At that time, the sun and the satellite are almost aligned and the
612 scattering angle (fig. [13d](#)) reaches values larger than 175° which corresponds to the region
613 where the glory phenomenon is typically observed. Several reasons can explain why the
614 retrieval does not perform well in backscattering direction. The first one is the uncertainty in
615 the LUT due to the truncation of the cloud phase function. Although the TMS correction gives
616 good results, biases still remain in the glory aureole (Iwabushi and Suzuki, 2009). Also, the
617 radiances in the glory are more sensitive to the cloud droplet microphysics (Mayer et al., 2004).
618 The assumption on the variance of the droplet size distribution may induce biases in the
619 retrieval. Therefore, the accuracy of the retrieval cannot be guaranteed within the glory aureole
620 and these observations should be discarded. In Figure [13](#), the timespans corresponding to the
621 MODIS Aqua and Terra overpasses in the region are highlighted in orange. This shows that
622 MODIS measurements are typically performed before and after SEVIRI observes the glory
623 backscattering over the SEAO, usually allowing comparisons between these instruments.

624
625 [The performance of the algorithm is further assessed by evaluating the stability of the retrieved](#)
626 [above-cloud AOT at pixel level. As noted by Chang and Christopher \(2016\), in this region over](#)
627 [these scales, aerosols are expected to have a limited temporal variability and the variation of](#)
628 [the above-cloud AOT is expected to be small between t=0 and t+/-15 minutes. The differences](#)
629 [between the AOT retrieved at t=0 and the running mean estimated between t-15 and t+15](#)
630 [minutes have been calculated at pixel level for observations between 09:00-15:00 UTC,](#)
631 [removing measurements within the glory backscattering region. Figure 14 shows the histogram](#)
632 [of the AOT differences calculated over a 12-day period \(01 to 12 September 2017\). The](#)
633 [differences follow a normal distribution centred around 0.0 with a standard deviation of 0.1.](#)
634 [This short-term variability can be attributed to several sources of uncertainties, such as the total](#)
635 [amount of water vapour, its vertical distribution, the retrieved cloud top height and the](#)
636 [numerical fitting procedure. This analysis indicates that the retrieval of the above-cloud AOT](#)
637 [remains relatively stable, with an observed variability of +/-0.1 between consecutive](#)
638 [observations. Except for the glory backscattering, the stability observed on the retrieved aerosol](#)
639 and cloud properties reinforces the reliability of the algorithm.

Deleted: .

Deleted: 12a

Deleted: that can be expressed as a linear trend. In order to assess the variability of the retrieved AOT, the linear trend +/- 2 times the standard deviation have been plotted on figure 12a (dashed lines).

Deleted: 15pm

Deleted: 12d

Deleted: 12

Deleted: Except from

650

651 **5. Conclusion**

652

653 Recently, progress has been made in the remote sensing field in order to fill the lack of aerosol
654 above cloud observations. Techniques have been developed to retrieve aerosol and cloud
655 properties over the SEAO from passive remote sensing instruments. These algorithms take
656 advantage of the colour-ratio effect (Jethva et al., 2013), which is the spectral contrast produced
657 by the aerosol absorption above clouds. Although OMI (Torres et al., 2012), MODIS (Jethva
658 et al., 2013; Meyer et al., 2015) and POLDER (Peers et al., 2015) already provide useful
659 information about aerosols above clouds, these instruments are on polar-orbiting satellites and
660 their low temporal resolutions prevent monitoring the diurnal variation of the cloud cover and
661 of the DRE of aerosols over the SEAO. For the first time, we have applied a similar algorithm
662 to geostationary measurements from the SEVIRI instrument, which has a repeat cycle of 15
663 minutes. The method consists of a LUT approach, using the channels at 0.64, 0.81 and 1.64
664 μm in order to retrieve simultaneously the above-cloud AOT, COT and CER.

Deleted: in

665

666 Compared to other satellite instruments, the SEVIRI measurements are more sensitive to the
667 absorption from atmospheric gases because of their wider spectral bands. Therefore, an
668 efficient atmospheric correction scheme is essential in order to separate the absorption from
669 aerosol absorption and from the atmospheric. Atmospheric transmittances are calculated with
670 the fast-radiative transfer model RTTOV based on the cloud top height observed by SEVIRI
671 and the forecasted water vapour profiles from the Met Office Unified Model. The water vapour
672 correction has the largest impact on the above-cloud aerosol retrieval. The impact of errors in
673 the atmospheric correction has been evaluated by modulating the humidity profile for a case
674 study. A positive bias of both the AOT and the COT is observed when the water vapour is
675 overestimated, and vice versa. On average, an 18.5% bias on the AOT and a 5.5% bias on the
676 COT are expected for a 10% error on the water vapour profile. Although a good accuracy is
677 expected from the forecast model, this limitation should be kept in mind when utilising or
678 further developing SEVIRI products. In the companion paper, the humidity from the forecast
679 will be compared against the dropsonde measurements from the CLARIFY-2017 campaign.

Deleted: the

Deleted: gas contribution

680

681 The choice of the aerosol model used to produce the LUT is also a key feature of the method.
682 *In situ* measurements of aerosols above clouds have been performed off the coast of Ascension
683 Island during the CLARIFY-2017 field campaign. An aerosol model optimised for the SEVIRI
684 spectral bands has been obtained by analysing the vertical profiles of extinction and absorption
685 from EXSCALABAR together with the size distribution from a PCASP. A bimodal lognormal
686 distribution has shown to adequately reproduce the observations. A fine mode radius of 0.12
687 μm has been obtained, which is in good agreement with the biomass burning measured over
688 the SEAO during SAFARI 2000 (Haywood et al., 2003). The refractive index has been
689 evaluated at 1.51-0.029i. The corresponding SSA of 0.85 at 0.55 μm is consistent with both *in*
690 *situ* and remote sensing observations of African biomass burning aerosols (Johnson et al., 2008;
691 Sayer et al., 2014). In addition to the uncertainty associated with the estimation of the aerosol
692 model, a seasonal dependence is expected in the biomass burning properties as well as

696 modifications due to aging processes during their transport over the SEAO. We have evaluated
 697 the impact of applying a single model assumption on both aerosol and cloud properties.
 698 Retrievals have been performed considering aerosol models with modified SSA and
 699 asymmetry factor g. It has been shown that the sensitivity of the retrieved cloud properties to
 700 the aerosol model assumption is small with errors lower than 5.6% on the COT and 2.6% on
 701 the CER. As expected the impact of the assumed aerosol properties is much larger on the above
 702 cloud AOT, with an uncertainty estimated at 40% before 15:00 UTC. This uncertainty is led
 703 by the sensitivity of the retrieval to the SSA. Because the method relies on the impact of the
 704 aerosol absorption on the light reflected by the clouds, the perturbation of the SSA has
 705 primarily an impact on the scattering contribution of the AOT. Therefore, a better accuracy is
 706 obtained on the retrieved AAOT, with biases generally lower than 17% before 15:00 UTC.
 707 After that time, an increase of the uncertainty on both the AOT and the AAOT has been
 708 observed, and users are advised to be careful when using the late afternoon aerosol product.
 709 For any satellite retrievals based on the colour-ratio technique, aerosol properties, including
 710 the SSA, have to be assumed and the same order of magnitude can be expected on the
 711 sensitivity of their AOT. This analysis highlights the importance of a suitable constrain on the
 712 SSA.

713
 714 Despite the wider channels and the narrower spectral range of SEVIRI, it has been
 715 demonstrated that the geostationary instrument has the potential to detect and quantify the
 716 absorbing aerosol plumes transported above the clouds of the SEAO. Except from observations
 717 within the glory backscattering for which the retrieval has shown to be unstable, a good
 718 consistency has been observed on the aerosol and cloud properties. The stability of the results
 719 during the day is promising for future uses of the SEVIRI algorithm. In the companion paper,
 720 the reliability of the retrieved aerosol and cloud properties will be further assessed by analysing
 721 the consistency with the MODIS retrievals and comparing with direct measurements from the
 722 CLARIFY-2017 field campaign. The potential of such a retrieval is obvious. The 15-minute
 723 resolution will aid in tracking the fate of above-cloud biomass burning aerosol and will prove
 724 invaluable for assessing models of the emission, transport and deposition of biomass burning
 725 aerosol, with implications for accurate determination of the direct radiative effects of biomass
 726 burning aerosol at high temporal resolution.

727
 728 **Author contribution**

729
 730 FP, PF and JMH developed the concept and the ideas for the conduction of this paper. PF
 731 implemented the atmospheric correction scheme and FP, the retrieval algorithm. CF, SJA, KS,
 732 MIC, NWD and JMH operated, calibrated and prepared the *in situ* measurements from
 733 EXSCALABAR and the PCASP. The reliability of the retrieved products was analysed
 734 throughout the development of the algorithm with the help of KGM and SEP. FP carried out
 735 the analysis and prepared the manuscript with contributions from all co-authors.
 736

- Deleted: size distributions
- Deleted: refractive indexes.
- Deleted: 3
- Deleted: model assumption
- Deleted: -
- Deleted: 31.2%. Owing to
- Deleted: to
- Deleted: above
- Deleted: an error of 6.1% only. This indicates
- Deleted: the estimated above-cloud AOT can be easily converted from one
- Deleted: model to another and that the results can be used to estimate the
- Deleted: DRE above clouds

- Deleted: NW
- Deleted: JM

753 **Acknowledgement**

754

755 This research was funded by the NERC CLARIFY project NE/L013479/1. Further support was
756 provided by the Research Council of Norway via the projects AC/BC (240372) and NetBC
757 (244141)

758

759 **References**

760 Aminou, D. M. A., Jacquet, B., and Pasternak, F.: Characteristics of the Meteosat
761 Second Generation (MSG) radiometer/imager: SEVIRI, Proc. SPIE, 3221, 3221 – 3221 – 13,
762 <https://doi.org/10.1117/12.298084>, 1997.

763
764 Brindley, H. and Ignatov, A.: Retrieval of mineral aerosol optical depth and size
765 information from Meteosat Second Generation SEVIRI solar reflectance bands, Remote
766 Sensing of Environment, 102, 344 – 363,
767 <https://doi.org/https://doi.org/10.1016/j.rse.2006.02.024>,
768 <http://www.sciencedirect.com/science/article/pii/S0034425706000952>, 2006.

769
770 Browell, E. V., Fenn, M. A., Butler, C. F., Grant, W. B., Clayton, M. B., Fishman, J.,
771 Bachmeier, A. S., Anderson, B. E., Gregory, G. L., Fuelberg, H. E., Bradshaw, J. D., Sandholm,
772 S. T., Blake, D. R., Heikes, B. G., Sachse, G. W., Singh, H. B., and Talbot, R. W.: Ozone and
773 aerosol distributions and air mass characteristics over the South Atlantic Basin during the
774 burning season, Journal of Geophysical Research: Atmospheres, 101, 24 043–24 068,
775 <https://doi.org/10.1029/95JD02536>, <https://agupubs.onlinelibrary.wiley.com/doi/abs/10.1029/95JD02536>, 1996.

776
777 Brown, A., Milton, S., Cullen, M., Golding, B., Mitchell, J., and Shelly, A.: Unified
778 Modeling and Prediction of Weather and Climate: A 25-Year Journey, Bulletin of the
779 American Meteorological Society, 93, 1865–1877, <https://doi.org/10.1175/BAMS-D-12-00018.1>, 2012.

780
781 Chang, I. and Christopher, S. A.: Identifying Absorbing Aerosols Above Clouds From
782 the Spinning Enhanced Visible and Infrared Imager Coupled With NASA A-Train Multiple
783 Sensors, IEEE Transactions on Geoscience and Remote Sensing, 54, 3163–3173,
784 <https://doi.org/10.1109/TGRS.2015.2513015>, 2016.

785
786 Clayton, A. M., Lorenc, A. C., and Barker, D. M.: Operational implementation of a
787 hybrid ensemble/4D-Var global data assimilation system at the Met Office, Quarterly Journal
788 of the Royal Meteorological Society, 139, 1445–1461, <https://doi.org/10.1002/qj.2054>,
789 <https://rmets.onlinelibrary.wiley.com/doi/abs/10.1002/qj.2054>, 2013.

790
791 [Cotterell, M. I., Orr-Ewing, A. J., Szpek, K., Haywood, J. M. and Langridge, J. M.: The
792 impact of bath gas composition on the calibration of photoacoustic spectrometers with ozone
793 at discrete visible wavelengths spanning the Chappuis band, Atmos. Meas. Tech., 12\(4\), 2371–
794 2385, doi:10.5194/amt-12-2371-2019, 2019.](https://doi.org/10.5194/amt-12-2371-2019)

795
796 Davies, N. W., Cotterell, M. I., Fox, C., Szpek, K., Haywood, J. M., and Langridge, J.
797 M.: On the accuracy of aerosol photoacoustic spectrometer calibrations using absorption by
798 ozone, Atmospheric Measurement Techniques, 11, 2313–2324, [https://doi.org/10.5194/amt-
799 11-2313-2018](https://doi.org/10.5194/amt-11-2313-2018), <https://www.atmos-meas-tech.net/11/2313/2018/>, 2018.

800
801 [Davies, N. W., Fox, C., Szpek, K., Cotterell, M. I., Taylor, J. W., Allan, J. D., Williams,
802 P. I., Trembath, J., Haywood, J. M., and Langridge, J. M.: Evaluating biases in filter-based
803 aerosol absorption measurements using photoacoustic spectroscopy, Atmos. Meas. Tech.
804 Discuss., <https://doi.org/10.5194/amt-2018-411>, in review, 2019.](https://doi.org/10.5194/amt-2018-411)

805
806 de Graaf, M., Tilstra, L. G., Wang, P., and Stammes, P.: Retrieval of the aerosol direct
807 radiative effect over clouds from spaceborne spectrometry, Journal of Geophysical Research:
808 Atmospheres, 117, <https://doi.org/10.1029/2011JD017160>, [https://agupubs.onlinelibrary.
809 wiley.com/doi/abs/10.1029/2011JD017160](https://agupubs.onlinelibrary.wiley.com/doi/abs/10.1029/2011JD017160), 2012.

Moved (insertion) [2]

804 de Haan, J. F., Bosma, P., and Hovenier, J.: The adding method for multiple scattering
805 calculations of polarized light, *Astronomy and Astrophysics*, 183, 371–391, 1987.

806 Eck, T. F., Holben, B. N., Ward, D. E., Mukelabai, M. M., Dubovik, O., Smirnov, A.,
807 Schafer, J. S., Hsu, N. C., Piketh, S. J., Queface, A., Roux, J. L., Swap, R. J., and Slutsker, I.:
808 Variability of biomass burning aerosol optical characteristics in southern Africa during the
809 SAFARI 2000 dry season campaign and a comparison of single scattering albedo estimates
810 from radiometric measurements, *Journal of Geophysical Research: Atmospheres*, 108,
811 <https://doi.org/10.1029/2002JD002321>, <https://agupubs.onlinelibrary.wiley.com/doi/abs/10.1029/2002JD002321>, 2003.

813 Edwards, J. M. and Slingo, A.: Studies with a flexible new radiation code. I: Choosing
814 a configuration for a large-scale model, *Quarterly Journal of the Royal Meteorological Society*,
815 122, 689–719, <https://doi.org/10.1002/qj.49712253107>, <https://rmets.onlinelibrary.wiley.com/doi/abs/10.1002/qj.49712253107>, 1996.

817 Francis, P. N., Hocking, J. A., and Saunders, R. W.: Improved diagnosis of low-level
818 cloud from MSG SEVIRI data for assimilation into Met Office limited area models, in:
819 *Proceedings of the 2008 EUMETSAT Meteorological Satellite Conference*, Darmstadt, 2008.

820 Gordon, H., Field, P. R., Abel, S. J., Dalvi, M., Grosvenor, D. P., Hill, A. A., Johnson,
821 B. T., Miltenberger, A. K., Yoshioka, M., and Carslaw, K. S.: Large simulated radiative effects
822 of smoke in the south-east Atlantic, *Atmospheric Chemistry and Physics*, 18, 15 261– 15 289,
823 <https://doi.org/10.5194/acp-18-15261-2018>, <https://www.atmos-chem-phys.net/18/15261/2018/>, 2018.

825 Hamann, U., Walther, A., Baum, B., Bennartz, R., Bugliaro, L., Derrien, M., Francis, P.
826 N., Heidinger, A., Joro, S., Kniffka, A., Le Gleau, H., Lockhoff, M., Lutz, H. J., Meirink, J. F.,
827 Minnis, P., Palikonda, R., Roebeling, R., Thoss, A., Platnick, S., Watts, P., and Wind, G.:
828 Remote sensing of cloud top pressure/height from SEVIRI : analysis of ten current retrieval
829 algorithms, *Atmospheric Measurement Techniques*, 7, 2839–2867,
830 <https://doi.org/10.5194/amt-7-2839-2014>, 2014.

831 Haywood, J. M., Osborne, S. R., Francis, P. N., Keil, A., Formenti, P., Andreae, M. O.,
832 and Kaye, P. H.: The mean physical and optical properties of regional haze dominated by
833 biomass burning aerosol measured from the C-130 aircraft during SAFARI 2000, *Journal of*
834 *Geophysical Research: Atmospheres*, 108, <https://doi.org/10.1029/2002JD002226>,
835 <https://agupubs.onlinelibrary.wiley.com/doi/abs/10.1029/2002JD002226>, 2003.

836 Haywood, J. M., Osborne, S. R., and Abel, S. J.: The effect of overlying absorbing
837 aerosol layers on remote sensing retrievals of cloud effective radius and cloud optical depth,
838 *Quarterly Journal of the Royal Meteorological Society*, 130, 779–800,
839 <https://doi.org/10.1256/qj.03.100>,
840 <https://rmets.onlinelibrary.wiley.com/doi/abs/10.1256/qj.03.100>, 2004.

841 Herman, M., Deuzé, J.-L., Marchand, A., Roger, B., and Lallart, P.: Aerosol remote
842 sensing from POLDER/ADEOS over the ocean: Improved retrieval using a nonspherical
843 particle model, *Journal of Geophysical Research: Atmospheres*, 110,
844 <https://doi.org/10.1029/2004JD004798>,
845 <https://agupubs.onlinelibrary.wiley.com/doi/abs/10.1029/2004JD004798>, 2005.

846 Hocking, J., Rayer, P., Rundle, D., Saunders, R., Matricardi, M., Geer, A., Brunel, P.,
847 and Vidot, J.: RTTOV v11 Users Guide, NWP-SAF Report; Met Office: Exeter, UK, 2014.

848 Iwabuchi, H. and Suzuki, T.: Fast and accurate radiance calculations using truncation
849 approximation for anisotropic scattering phase functions, *Journal of Quantitative Spectroscopy*

850 and Radiative Transfer, 110, 1926 – 1939,
851 <https://doi.org/https://doi.org/10.1016/j.jqsrt.2009.04.006>,
852 <http://www.sciencedirect.com/science/article/pii/S0022407309001496>, 2009.

853 Jethva, H., Torres, O., Remer, L. A., and Bhartia, P. K.: A Color Ratio Method for
854 Simultaneous Retrieval of Aerosol and Cloud Optical Thickness of Above-Cloud Absorbing
855 Aerosols From Passive Sensors: Application to MODIS Measurements, IEEE Transactions on
856 Geoscience and Remote Sensing, 51, 3862 – 3870,
857 <https://doi.org/10.1109/TGRS.2012.2230008>, 2013.

858 Johnson, B. T., Osborne, S. R., Haywood, J. M., and Harrison, M. A. J.: Aircraft
859 measurements of biomass burning aerosol over West Africa during DABEX, Journal of
860 Geophysical Research: Atmospheres, 113, <https://doi.org/10.1029/2007JD009451>,
861 <https://agupubs.onlinelibrary.wiley.com/doi/abs/10.1029/2007JD009451>, 2008.

862 Keil, A. and Haywood, J. M.: Solar radiative forcing by biomass burning aerosol
863 particles during SAFARI 2000: A case study based on measured aerosol and cloud properties,
864 Journal of Geophysical Research: Atmospheres, 108, <https://doi.org/10.1029/2002JD002315>,
865 <https://agupubs.onlinelibrary.wiley.com/doi/abs/10.1029/2002JD002315>, 2003.

866 Koppmann, R., von Czapiewski, K., and Reid, J. S.: A review of biomass burning
867 emissions, part I: gaseous emissions of carbon monoxide, methane, volatile organic
868 compounds, and nitrogen containing compounds, Atmospheric Chemistry and Physics
869 Discussions, 5, 10 455–10 516, <https://doi.org/10.5194/acpd-5-10455-2005>,
870 <https://www.atmos-chem-phys-discuss.net/5/10455/2005/>, 2005.

871 Koren, I., Kaufman, Y. J., Remer, L. A., and Martins, J. V.: Measurement of the Effect
872 of Amazon Smoke on Inhibition of Cloud Formation, Science, 303, 1342–1345,
873 <https://doi.org/10.1126/science.1089424>,
874 <http://science.sciencemag.org/content/303/5662/1342>, 2004.

875 Levy, R. C., Remer, L. A., Tanre, D., Mattoo, S., and Kaufman, Y. J.: Algorithm for
876 remote sensing of tropospheric aerosol over dark targets from MODIS: Collections 005 and
877 051: Revision 2; Feb 2009, MODIS algorithm theoretical basis document, 2009.

878 Lu, Z., Liu, X., Zhang, Z., Zhao, C., Meyer, K., Rajapakshe, C., Wu, C., Yang, Z., and
879 Penner, J. E.: Biomass smoke from southern Africa can significantly enhance the brightness of
880 stratocumulus over the southeastern Atlantic Ocean, Proceedings of the National Academy of
881 Sciences, 115, 2924–2929, <https://doi.org/10.1073/pnas.1713703115>,
882 <https://www.pnas.org/content/115/12/2924>, 2018.

883 Magi, B. I. and Hobbs, P. V.: Effects of humidity on aerosols in southern Africa during
884 the biomass burning season, Journal of Geophysical Research: Atmospheres, 108,
885 <https://doi.org/10.1029/2002JD002144>, [https://agupubs.onlinelibrary.wiley.com/doi/abs/10.](https://agupubs.onlinelibrary.wiley.com/doi/abs/10.1029/2002JD002144)
886 [1029/2002JD002144](https://agupubs.onlinelibrary.wiley.com/doi/abs/10.1029/2002JD002144), 2003.

887 Manners, J.: Socrates technical guide suite of community radiative transfer codes based
888 on edwards and slingo, in: Tech. Rep., Met Office, FitzRoy Rd, Exeter EX1 3PB, 2015.

889 [Martins, J. V., Hobbs, P. V., Weiss, R. E., and Artaxo, P., Sphericity and morphology](#)
890 [of smoke particles from biomass burning in Brazil, Journal of Geophysical Research, 103\(](#)
891 [D24\), 32051– 32057, doi:10.1029/98JD01153, 1998.](#)

892 Matricardi, M.: The generation of RTTOV regression coefficients for IASI and AIRS
893 using a new profile training set and a new line-by-line database, European Centre for Medium-
894 Range Weather Forecasts, 2008.

895 Matricardi, M., Chevallier, F., Kelly, G., and Thépaut, J.-N.: An improved general fast
896 radiative transfer model for the assimilation of radiance observations, *Quarterly Journal of the*
897 *Royal Meteorological Society*, 130, 153–173, <https://doi.org/10.1256/qj.02.181>, <https://rmets.onlinelibrary.wiley.com/doi/abs/10.1256/qj.02.181>, 2004.

899 Mayer, B., Schröder, M., Preusker, R., and Schüller, L.: Remote sensing of water cloud
900 droplet size distributions using the backscatter glory: a case study, *Atmospheric Chemistry and*
901 *Physics*, 4, 1255–1263, <https://doi.org/10.5194/acp-4-1255-2004>, <https://www.atmos-chem-phys.net/4/1255/2004/>, 2004.

903 McClatchey, R. A., Fenn, R. W., Selby, J. A., Volz, F., and Garing, J.: Optical properties
904 of the atmosphere, Tech. rep., Air Force Cambridge Research Labs Hanscom AFB MA, 1972.

905 Meyer, K., Platnick, S., and Zhang, Z.: Simultaneously inferring above-cloud absorbing
906 aerosol optical thickness and underlying liquid phase cloud optical and microphysical
907 properties using MODIS, *Journal of Geophysical Research: Atmospheres*, 120, 5524–5547,
908 <https://doi.org/10.1002/2015JD023128>,
909 <https://agupubs.onlinelibrary.wiley.com/doi/abs/10.1002/2015JD023128>, 2015.

910 Min, M. and Zhang, Z.: On the influence of cloud fraction diurnal cycle and sub-grid
911 cloud optical thickness variability on all-sky direct aerosol radiative forcing, *Journal of*
912 *Quantitative Spectroscopy and Radiative Transfer*, 142, 25 – 36,
913 <https://doi.org/https://doi.org/10.1016/j.jqsrt.2014.03.014>,
914 <http://www.sciencedirect.com/science/article/pii/S0022407314001307>, 2014.

915 Nakajima, T. and King, M. D.: Determination of the Optical Thickness and Effective
916 Particle Radius of Clouds from Reflected Solar Radiation Measurements. Part I: Theory,
917 *Journal of the Atmospheric Sciences*, 47, 1878–1893, [https://doi.org/10.1175/1520-0469\(1990\)047<1878:DOTOTA>2.0.CO;2](https://doi.org/10.1175/1520-0469(1990)047<1878:DOTOTA>2.0.CO;2), 1990.

919 Nakajima, T. and Tanaka, M.: Algorithms for radiative intensity calculations in
920 moderately thick atmospheres using a truncation approximation, *Journal of Quantitative*
921 *Spectroscopy and Radiative Transfer*, 40, 51 – 69, [https://doi.org/https://doi.org/10.1016/0022-4073\(88\)90031-3](https://doi.org/https://doi.org/10.1016/0022-4073(88)90031-3),
922 <http://www.sciencedirect.com/science/article/pii/0022407388900313>,
923 1988.

924 Peers, F., Waquet, F., Cornet, C., Dubuisson, P., Ducos, F., Goloub, P., Szczap, F.,
925 Tanré, D., and Thieuleux, F.: Absorption of aerosols above clouds from POLDER/PARASOL
926 measurements and estimation of their direct radiative effect, *Atmospheric Chemistry and*
927 *Physics*, 15, 4179–4196, <https://doi.org/10.5194/acp-15-4179-2015>, <https://www.atmos-chem-phys.net/15/4179/2015/>, 2015.

929 Peers, F., Bellouin, N., Waquet, F., Ducos, F., Goloub, P., Mollard, J., Myhre, G., Skeie,
930 R. B., Takemura, T., Tanré, D., Thieuleux, F., and Zhang, K.: Comparison of aerosol optical
931 properties above clouds between POLDER and AeroCom models over the South East Atlantic
932 Ocean during the fire season, *Geophysical Research Letters*, 43, 3991–4000,
933 <https://doi.org/10.1002/2016GL068222>,
934 <https://agupubs.onlinelibrary.wiley.com/doi/abs/10.1002/2016GL068222>, 2016.

935 Platnick, S.: [Vertical photon transport in cloud remote sensing problems](#), *Journal of*
936 *Geophysical Research*, 105, 22 919–22 935, 2000.

937 Rosenberg, P. D., Dean, A. R., Williams, P. I., Dorsey, J. R., Minikin, A., Pickering, M.
938 A., and Petzold, A.: Particle sizing calibration with refractive index correction for light
939 scattering optical particle counters and impacts upon PCASP and CDP data collected during
940 the Fennec campaign, *Atmospheric Measurement Techniques*, 5, 1147–1163,

Deleted: Ackerman, S., King, M., Meyer, K., Menzel,

Moved up [2]: W.,

Deleted: Holz, R., Baum, B., and Yang, P.: MODIS atmosphere L2 cloud product (06_L2), NASA MODIS Adaptive Processing System, Goddard Space Flight Center, 2015.

947 <https://doi.org/10.5194/amt-5-1147-2012>, <https://www.atmos-meas-tech.net/5/1147/2012/>,
948 2012.

949 Rosenfeld, D.: Suppression of Rain and Snow by Urban and Industrial Air Pollution,
950 Science, 287, 1793–1796, <https://doi.org/10.1126/science.287.5459.1793>,
951 <http://science.sciencemag.org/content/287/5459/1793>, 2000.

952 Sayer, A. M., Hsu, N. C., Eck, T. F., Smirnov, A., and Holben, B. N.: AERONET-based
953 models of smoke-dominated aerosol near source regions and transported over oceans, and
954 implications for satellite retrievals of aerosol optical depth, Atmospheric Chemistry and
955 Physics, 14, 11 493–11 523, <https://doi.org/10.5194/acp-14-11493-2014>, <https://www.atmos-chem-phys.net/14/11493/2014/>, 2014.

957 [Szczerzak, M., Austin, P. H. and Krummel, P. B.: Variability of Optical Depth and](https://doi.org/10.1175/1520-0469(2001)058<2912:VOODAE>2.0.CO;2)
958 [Effective Radius in Marine Stratocumulus Clouds, J. Atmos. Sci., 58\(19\), 2912–2926,](https://doi.org/10.1175/1520-0469(2001)058<2912:VOODAE>2.0.CO;2)
959 [doi:10.1175/1520-0469\(2001\)058<2912:VOODAE>2.0.CO;2, 2001.](https://doi.org/10.1175/1520-0469(2001)058<2912:VOODAE>2.0.CO;2)

960 Thieuleux, F., Moulin, C., Bréon, F. M., Maignan, F., Poitou, J., and Tanré, D.: Remote
961 sensing of aerosols over the oceans using MSG/SEVIRI imagery, Annales Geophysicae, 23,
962 3561–3568, <https://doi.org/10.5194/angeo-23-3561-2005>, 2005.

963 Torres, O., Jethva, H., and Bhartia, P. K.: Retrieval of Aerosol Optical Depth above
964 Clouds from OMI Observations: Sensitivity Analysis and Case Studies, Journal of the
965 Atmospheric Sciences, 69, 1037–1053, <https://doi.org/10.1175/JAS-D-11-0130.1>, 2012.

966 Twomey, S.: Pollution and the planetary albedo, Atmospheric Environment (1967), 8,
967 1251 – 1256, [https://doi.org/10.1016/0004-6981\(74\)90004-3](https://doi.org/10.1016/0004-6981(74)90004-3),
968 <http://www.sciencedirect.com/science/article/pii/0004698174900043>, 1974.

969 Waquet, F., Cornet, C., Deuzé, J.-L., Dubovik, O., Ducos, F., Goloub, P., Herman, M.,
970 Lapyonok, T., Labonnote, L. C., Riedi, J., Tanré, D., Thieuleux, F., and Vanbauce, C.:
971 Retrieval of aerosol microphysical and optical properties above liquid clouds from
972 POLDER/PARASOL polarization measurements, Atmospheric Measurement Techniques, 6,
973 991–1016, <https://doi.org/10.5194/amt-6-991-2013>, <https://www.atmos-meas-tech.net/6/991/2013/>, 2013a.

975 Waquet, F., Peers, F., Ducos, F., Goloub, P., Platnick, S., Riedi, J., Tanré, D., and
976 Thieuleux, F.: Global analysis of aerosol properties above clouds, Geophysical Research
977 Letters, 40, 5809–5814, <https://doi.org/10.1002/2013GL057482>, <https://agupubs.onlinelibrary.wiley.com/doi/abs/10.1002/2013GL057482>, 2013b.

979 Watts, P., Mutlow, C., Baran, A., and Zavody, A.: Study on cloud properties derived
980 from Meteosat Second Generation observations, EUMETSAT ITT, 97, 181, 1998.

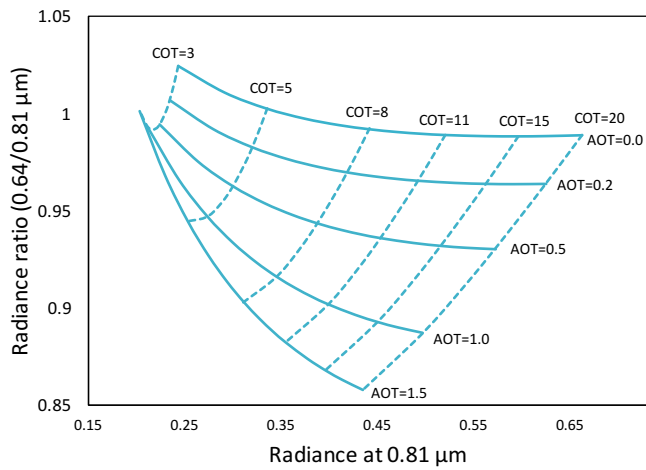
981 Wilcox, E. M.: Stratocumulus cloud thickening beneath layers of absorbing smoke
982 aerosol, Atmospheric Chemistry and Physics, 10, 11 769–11 777, <https://doi.org/10.5194/acp-10-11769-2010>, <https://www.atmos-chem-phys.net/10/11769/2010/>, 2010.

984 Wilcox, E. M.: Direct and semi-direct radiative forcing of smoke aerosols over clouds,
985 Atmospheric Chemistry and Physics, 12, 139–149, <https://doi.org/10.5194/acp-12-139-2012>,
986 <https://www.atmos-chem-phys.net/12/139/2012/>, 2012.

987 Wiscombe, W.: The Delta–M method: Rapid yet accurate radiative flux calculations for
988 strongly asymmetric phase functions, Journal of the atmospheric sciences, 34, 1408–1422,
989 1977.

990 Zuidema, P., Redemann, J., Haywood, J., Wood, R., Piketh, S., Hipondoka, M., and
991 Formenti, P.: Smoke and Clouds above the Southeast Atlantic: Upcoming Field Campaigns
992 Probe Absorbing Aerosol's Impact on Climate, *Bulletin of the American Meteorological*
993 *Society*, 97, 1131–1135, <https://doi.org/10.1175/BAMS-D-15-00082.1>, 2016.

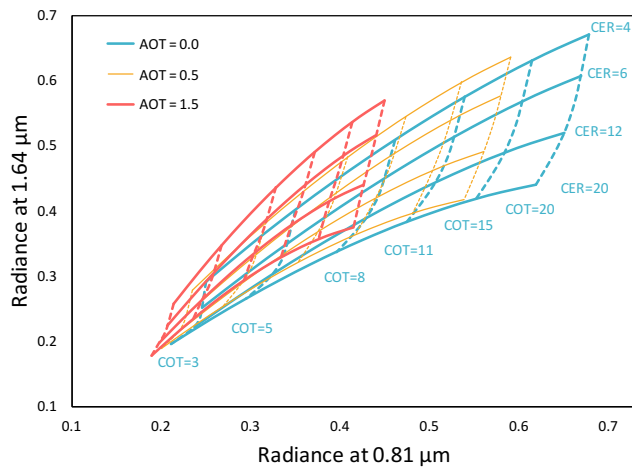
994 Zuidema, P., Sedlacek III, A. J., Flynn, C., Springston, S., Delgado, R., Zhang, J.,
995 Aiken, A. C., Koontz, A., and Muradyan, P.: The Ascension Island Boundary Layer in the
996 Remote Southeast Atlantic is Often Smoky, *Geophysical Research Letters*, 45, 4456–4465,
997 <https://doi.org/10.1002/2017GL076926>,
998 <https://agupubs.onlinelibrary.wiley.com/doi/abs/10.1002/2017GL076926>, 2018.



999
1000
1001
1002
1003

Figure 1: Radiance ratio $R_{0.64}/R_{0.81}$ as a function of the radiance at $0.81\mu\text{m}$ for absorbing aerosols above clouds simulated with the adding-doubling method (De Haan et al., 1987). COTs and AOTs are indicated at $0.55\mu\text{m}$.

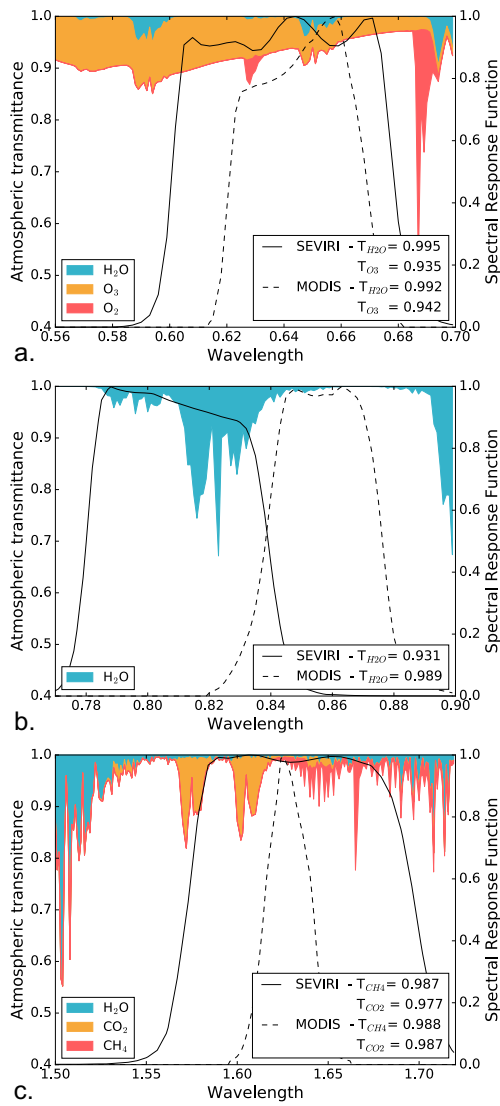
Deleted: Cloud optical thicknesses (COT) and aerosol optical thicknesses (AOT)



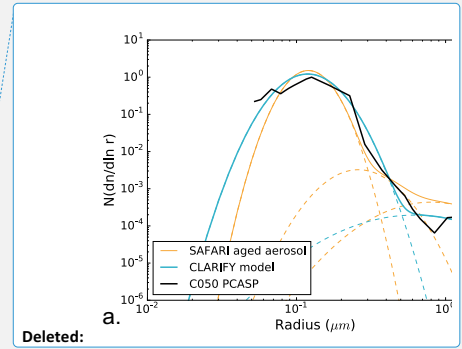
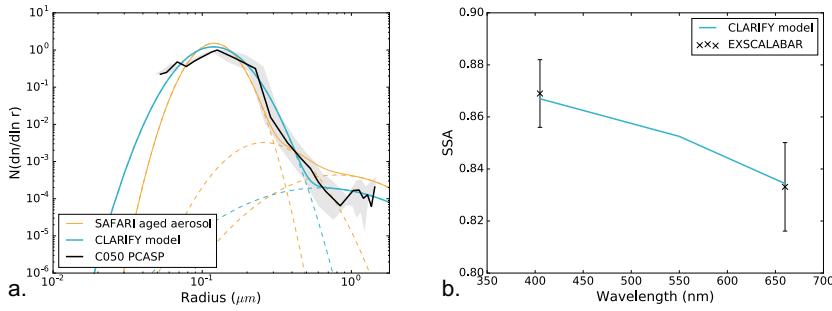
1004
1005
1006
1007
1008

Figure 2: Simulated radiances at $1.64\mu\text{m}$ and $0.81\mu\text{m}$ for clouds with varying COTs and CERs (in μm), without (blue) and with (orange and red) overlying absorbing aerosols above. The viewing geometry, the aerosol and the cloud properties are the same as Figure 1.

Deleted: COT
Deleted: CER



1013
 1014 **Figure 3:** Spectral response function of the SEVIRI bands at 0.64 (a), 0.81 (b) and 1.64 μm (c)
 1015 with the corresponding MODIS ones (dashed lines) as well as the atmospheric transmittance
 1016 within the spectral range (in colour). The transmittances have been calculated with the
 1017 SOCRATES radiative transfer scheme (Manners et al., 2015; Edwards and Slingo, 1996)
 1018 assuming a humidity profile measured during SAFARI (Keil and Haywood, 2003). In the
 1019 legend of each plot, the transmittance weighted by the spectral response function is given for
 1020 the main absorbing gases.



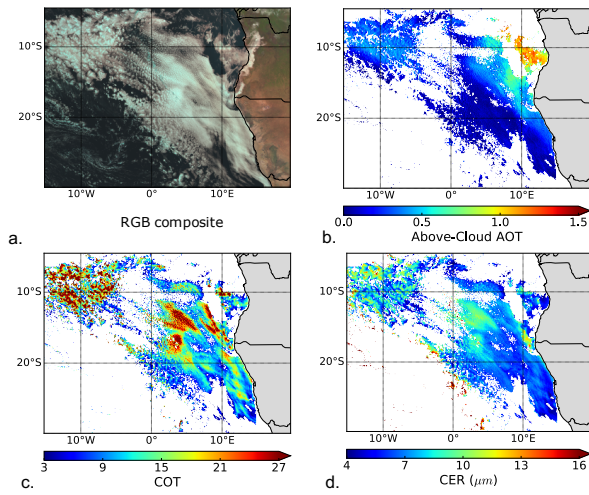
Deleted:

Deleted: ones

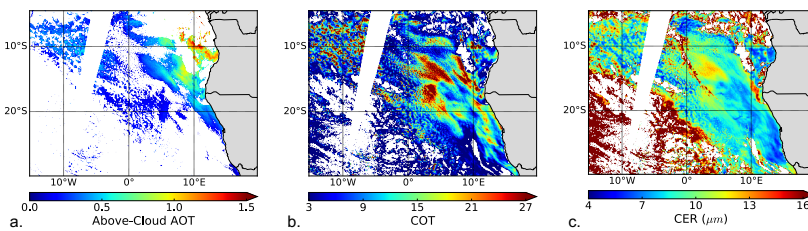
1021
1022 **Figure 4:** Normalized size distribution (a) and SSA (b) measured above clouds during flight
1023 C050 of the CLARIFY-2017 campaign (black). [The grey shade area represents the PCASP](#)
1024 [measurement and calibration uncertainties](#). Blue lines represent the fitted aerosol model, the
1025 orange lines correspond to the aged aerosol size distribution from SAFARI (Haywood et al.,
1026 2003), and the dashed lines shows the contribution of each mode. CLARIFY-2017 aerosol
1027 model: $[r_{\text{fine}}, \sigma_{\text{fine}}, N_{\text{fine}}; r_{\text{coarse}}, \sigma_{\text{coarse}}, N_{\text{coarse}}] = [0.12\mu\text{m}, 1.42, 0.9996; 0.62\mu\text{m}, 2.23, 0.0004]$,
1028 refractive index = $1.51 - 0.029i$. SAFARI aged aerosol model: $[r_1, \sigma_1, N_1; r_2, \sigma_2, N_2; r_3, \sigma_3, N_3]$
1029 = $[0.12\mu\text{m}, 1.30, 0.996; 0.26\mu\text{m}, 1.50, 0.0033; 0.80\mu\text{m}, 1.90, 0.0007]$.
1030

Aerosol model				
Size distribution	Bimodal lognormal distribution			
	$r_{\text{fine}} = 0.12 \mu\text{m}$	$\sigma_{\text{fine}} = 1.42$	$N_{\text{fine}} = 0.9996$	
	$r_{\text{coarse}} = 0.62 \mu\text{m}$	$\sigma_{\text{coarse}} = 2.23$	$N_{\text{coarse}} = 0.0004$	
Refractive index	$1.51 - 0.029i$			
Wavelength	$0.55 \mu\text{m}^*$	$0.64 \mu\text{m}$	$0.81 \mu\text{m}$	$1.64 \mu\text{m}$
SSA	0.852	0.839	0.804	0.643
g	0.649	0.612	0.538	0.468
Cloud model				
Size distribution	Gamma law			
	r_{eff} from 4 to 60 μm		$v_{\text{eff}} = 0.06$	

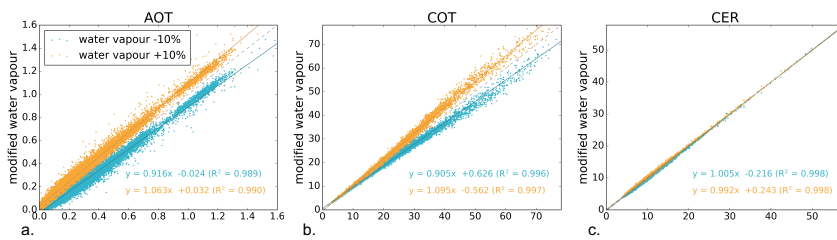
1031 **Table 1:** Aerosol and cloud properties used to compute the radiances LUT of the SEVIRI
1032 retrieval. (* Note that $0.55\mu\text{m}$ does not correspond to a SEVIRI channel.)
1033



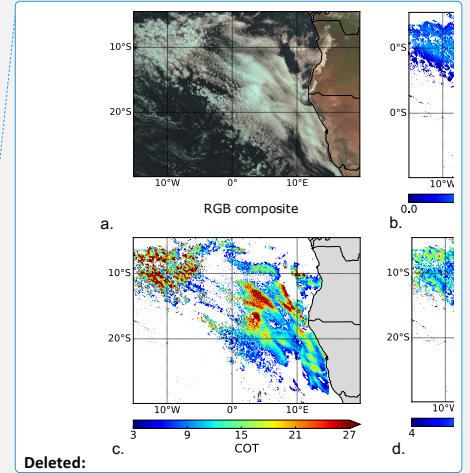
1036
1037 **Figure 5:** RGB composite (a), Above cloud AOT at $0.55 \mu\text{m}$ (b) and cloud properties (c and
1038 d) retrieved from SEVIRI measurements on the 28 August 2017 at 10:12 UTC over the SEAO.
1039



1040
1041 **Figure 6:** Above cloud AOT at $0.55 \mu\text{m}$ (a) and cloud properties (b and c) retrieved from
1042 MODIS-Terra with the MOD06ACAERO algorithm (Meyer et al., 2015) on the 28 August
1043 2017.
1044

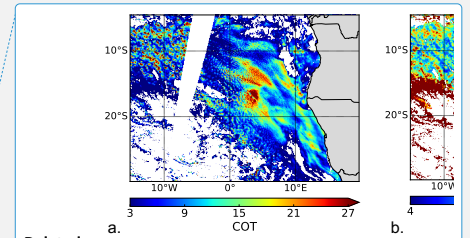


1045
1046 **Figure 7:** Uncertainty in the retrieved above-cloud AOT (a), COT (b) and CER(c) due to an
1047 error of +10% in orange and -10% in blue on the specific humidity profile compare to the
1048 original forecast for 28 August 2017 at 10:12 UTC.
1049



Deleted:

Deleted: 550 nm



Deleted:

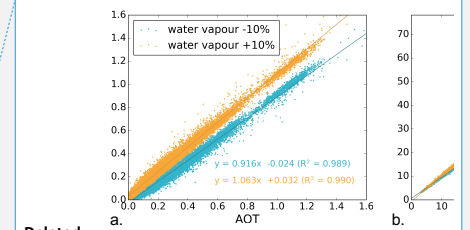
Deleted: Cloud Optical Thickness (COT

Deleted: droplet effective radius (CER)

Deleted: the

Deleted: Collection 6 for

Deleted: (Platnick et al., 2015).

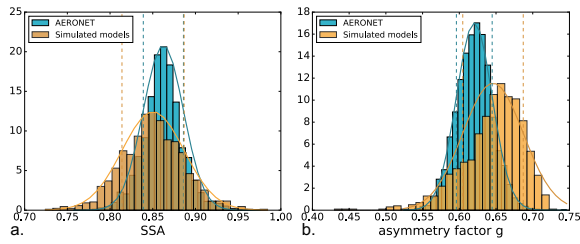


Deleted:

Deleted: water vapour

Deleted: the

1061
1062



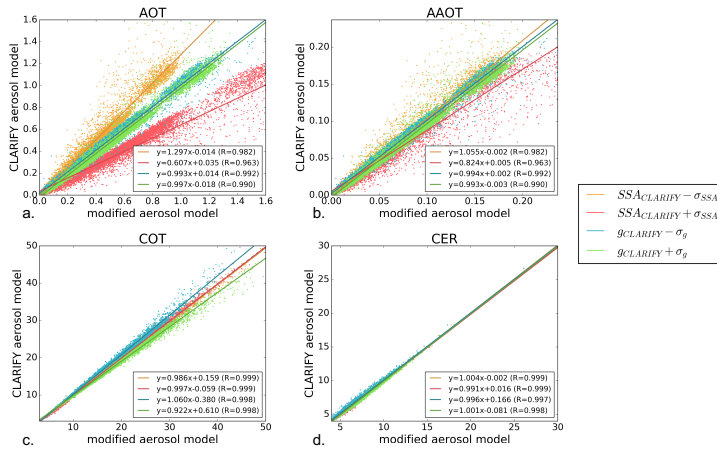
1063
1064
1065
1066
1067

Figure 8: Histograms of the SSA (a) and asymmetry factor g (b) at $0.55 \mu\text{m}$ simulated from a range of size distribution and refractive index (orange) and retrieved by AERONET (blue) over the Southern Africa. Dashed lines represent the mean \pm the standard deviation.

Model	SSA	g	r_{fine}	σ_{fine}	refr. index
CLARIFY	0.852	0.649	0.12	1.42	1.51-0.029i
$SSA_{\text{CLARIFY}} - \sigma_{\text{SSA}}$	0.812	0.648	0.12	1.42	1.51-0.037i
$SSA_{\text{CLARIFY}} + \sigma_{\text{SSA}}$	0.891	0.649	0.12	1.42	1.52-0.021i
$g_{\text{CLARIFY}} - \sigma_g$	0.852	0.603	0.12	1.30	1.53-0.027i
$g_{\text{CLARIFY}} + \sigma_g$	0.851	0.686	0.12	1.51	1.50-0.030i
$SSA_{\text{CLARIFY}} - \sigma_{\text{SSA}}, g_{\text{CLARIFY}} - \sigma_g$	0.813	0.604	0.11	1.37	1.52-0.034i
$SSA_{\text{CLARIFY}} + \sigma_{\text{SSA}}, g_{\text{CLARIFY}} + \sigma_g$	0.886	0.687	0.13	1.50	1.49-0.022i
$SSA_{\text{CLARIFY}} - \sigma_{\text{SSA}}, g_{\text{CLARIFY}} + \sigma_g$	0.814	0.684	0.12	1.51	1.50-0.041i
$SSA_{\text{CLARIFY}} + \sigma_{\text{SSA}}, g_{\text{CLARIFY}} - \sigma_g$	0.884	0.602	0.11	1.36	1.49-0.017i

1068
1069
1070
1071

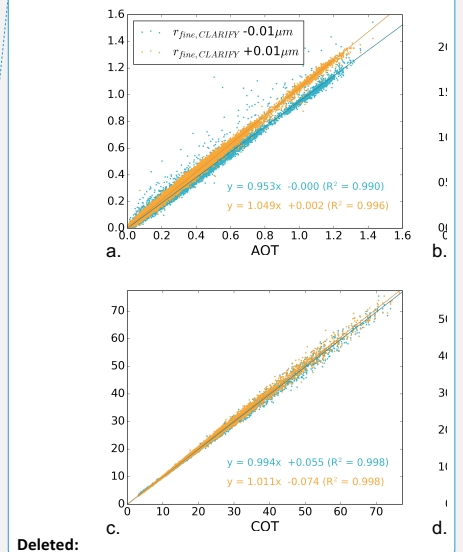
Table 2: Aerosol properties used to test the sensitivity of the SEVIRI to the aerosol model. SSA and g are given at $0.55 \mu\text{m}$.



1072

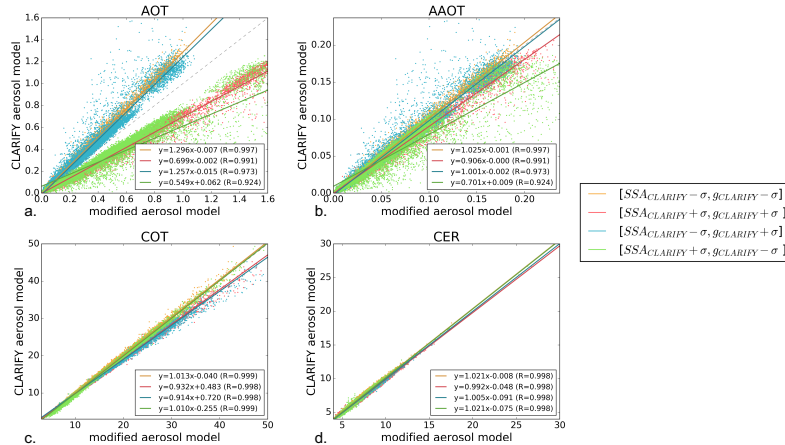
Formatted: Font:Bold

Deleted: retrieval and the corresponding differences Δ obtained on the above-cloud AOT, AAOT, COT and CER with respect to retrieved values using the unperturbed

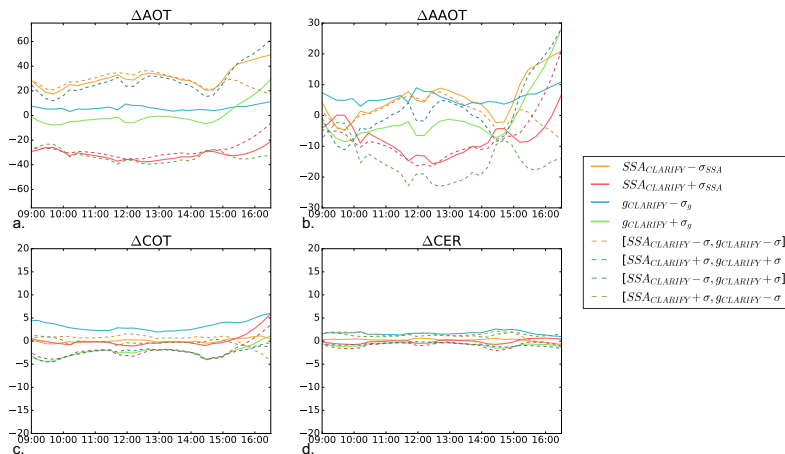


Deleted:

1077 **Figure 9:** Impact of the assumption on the SSA and the asymmetry factor g on the retrieved
 1078 aerosol and cloud properties. AOT, AAOT, COT and CER obtained for 28 August 2017 at
 1079 10:12 UTC with the CLARIFY-2017 model are plotted against the properties retrieved with
 1080 the modified aerosol models.
 1081

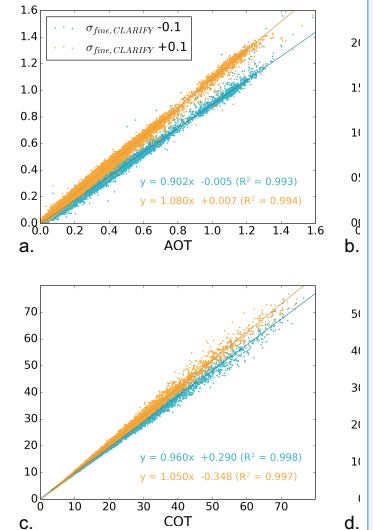


1082 **Figure 10:** Similar to Figure 9 for the combined impact of g and the SSA.
 1083
 1084



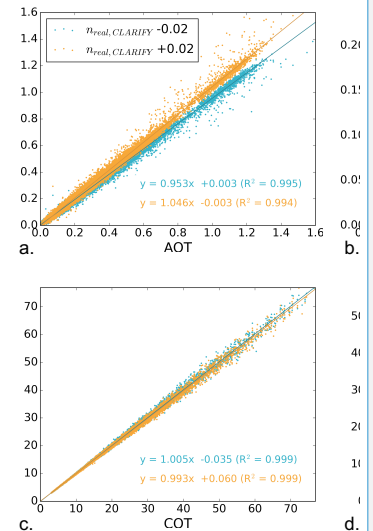
1085 **Figure 11:** Time series (UTC) of the difference Δ (in %) of the above-cloud AOT (a), AAOT
 1086 (b), COT (c), CER (d) retrieved with the CLARIFY model and the modified aerosol models
 1087 for the 28 August 2017.
 1088
 1089

Deleted: 8...: Impact of the assumption on the fine mode radius r_{fine} , SA and the asymmetry factor g on the retrieved aerosol and cloud properties. AOT, AAOT, COT and CER obtained for the 28 August 2017 at 10:12 UTC with the modified aerosol models... CLARIFY-2017 model are plotted against the properties retrieved with the CLARIFY-2017 model ... [2]



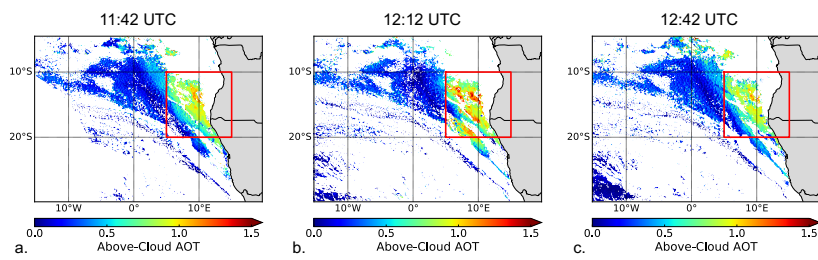
Deleted:

Deleted: 9...0: Similar to Figure 8... for the combined impact of the assumption on the fine mode standard deviation σ_{fine} ... [3]

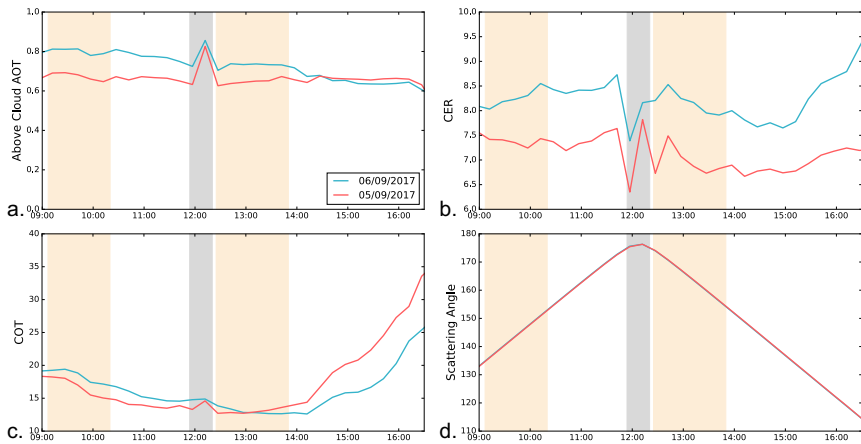


Deleted:

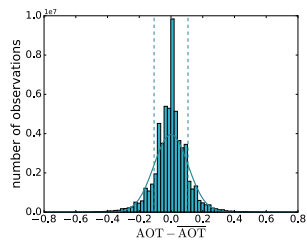
Deleted: 10: Similar to Figure 8 for the impact... 1: Time series (UTC) of the assumption on the real part... difference Δ (in %) of the above-cloud AOT (a), AAOT (b), COT (c), CER (d) retrieved with the CLARIFY model and the modified aerosol refractive index n_{real} ... [4]



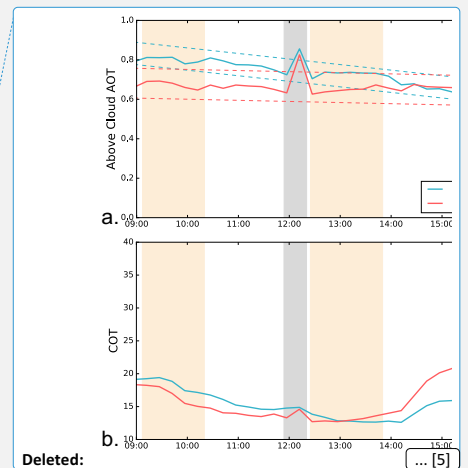
1135
1136 **Figure 12:** Above-cloud AOT retrieved the 05 September 2017 at 11:42, 12:12 and 12:42
1137 UTC. The red square represents the area over which the SEVIRI products have been averaged.
1138



1139
1140 **Figure 13:** Time series (UTC) of the above-cloud AOT (a), COT (b), CER(c) and scattering
1141 angle(d) averaged between 20°S and 10°S, and 5°E and 15°E for the 5th and 6th September
1142 2017. The grey area represents scattering angles larger than 175° and the orange areas show
1143 the typical overpass times of MODIS Aqua and Terra over the region.
1144



1145
1146 **Figure 14:** Histogram of the difference between AOT retrieved at $t=0$ and the running mean
1147 calculated between $t-15$ and $t+15$ minutes from 01 September to 12 September 2017.
1148 Observations within the glory region have been removed. Dashed lines represent the mean +/-
1149 the standard deviation.



Deleted:

Deleted: ones

Deleted: The

Deleted: in figure a corresponds to +/- 2 times

Figure 8 and 9 show the impact of a variation of $\pm 0.01 \mu\text{m}$ on the fine mode radius and ± 0.1 on the fine mode standard deviation. For each aerosol and cloud property, a linear relationship is observed between the retrieval using the standard CLARIFY-2017 aerosol model and the modified one. The aerosol size distribution has little influence on the retrieved cloud properties. On average, the modification of the fine mode standard deviation leads to a difference of 2.2% on the COT and 1.0% the CER. The effect associated with a change in the fine mode radius is even lower than 1%. As expected, the above-cloud AOT is more sensitive to the aerosol size distribution used for the inversion and differences up to 11.8% have been observed when the fine mode standard deviation is decreased by 0.1. However, the retrieval of the AOT is based on the detection of the aerosol absorption of the light reflected by the clouds. Therefore, the impact of an error on the aerosol size distribution on the AAOT retrieval is reduced to 5.4% for the standard deviation and 1.4% for the fine mode radius.

To assess the impact of the assumed aerosol refractive index on the retrieved aerosol and cloud properties of interest, variations of ± 0.02 and ± 0.008 have been applied to the real and imaginary parts of the refractive index, respectively. Figure 10 and 11 compare the retrieved aerosol and cloud properties from SEVIRI radiance data for the CLARIFY-2017 aerosol model with those retrieved when the aerosol refractive index parameters are perturbed. The influence of refractive index is similar to the one of the modified aerosol size distribution in that differences of $<1\%$ are observed in both COT and CER and a larger impact is found on the AOT with differences up to 39% where the imaginary refractive index is decreased by 0.008. The magnitude of the impact on the AOT is correlated to the difference of SSA between the CLARIFY-2017 and the perturbed aerosol model. Therefore, the retrieval of the AAOT is also less sensitive to the assumption on the aerosol refractive index, with an impact lower than 6.5%.

In order to evaluate the uncertainty u_{aer} of the retrieved aerosol and cloud properties due to the aerosol model assumptions, we combined the uncertainty u_i from the above sensitivity studies using:

The uncertainty has been estimated at 31.2% on the AOT, 2.3% on the COT and 1.2 % on the CER. Owing to the sensitivity of the retrieval to the aerosol absorption above clouds, a 6.1% uncertainty has been obtained on the AAOT, which is, together with the cloud albedo, the main parameter for the estimation of the DRE of absorbing aerosols above clouds.

8

8

8

8

8

Page 28: [3] Deleted Authors 09/05/2019 12:56:00

9

Page 28: [3] Deleted Authors 09/05/2019 12:56:00

9

Page 28: [3] Deleted Authors 09/05/2019 12:56:00

9

Page 28: [4] Deleted Authors 09/05/2019 12:56:00

10: Similar to Figure 8 for the impact

Page 28: [4] Deleted Authors 09/05/2019 12:56:00

10: Similar to Figure 8 for the impact

Page 28: [4] Deleted Authors 09/05/2019 12:56:00

10: Similar to Figure 8 for the impact

Page 28: [4] Deleted Authors 09/05/2019 12:56:00

10: Similar to Figure 8 for the impact

Page 29: [5] Deleted Authors 09/05/2019 12:56:00

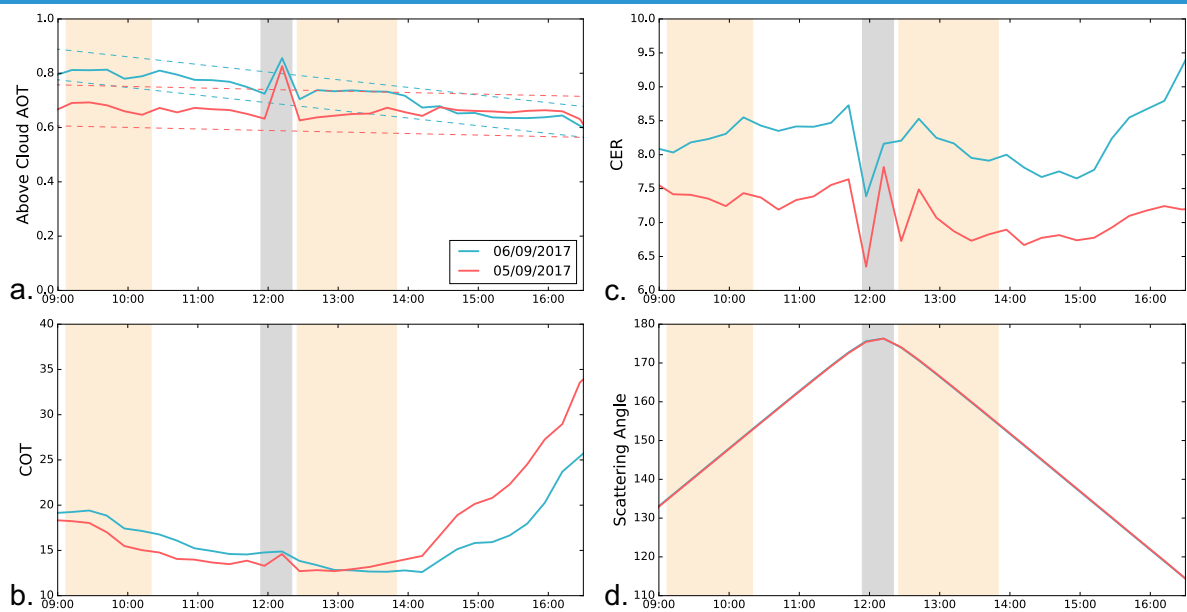


Figure 12: Time series